

An efficient multiscale multigrid preconditioner for Darcy flow in high-contrast media

Changqing Ye^a, Shubin Fu^{b,*}, Eric T. Chung^a, Jizu Huang^{c,d}

^aDepartment of Mathematics, The Chinese University of Hong Kong, Shatin, Hong Kong SAR

^bEastern Institute for Advanced Study, Ningbo, 315200, Zhejiang, PR China

^cLSEC, Academy of Mathematics and Systems Science, Chinese Academy of Sciences, Beijing, 100190, PR China

^dSchool of Mathematical Sciences, University of Chinese Academy of Sciences, Beijing, 100049, PR China

Abstract

In this paper, we develop a multigrid preconditioner to solve Darcy flow in highly heterogeneous porous media. The key component of the preconditioner is to construct a sequence of nested subspaces $W_{\mathcal{L}} \subset W_{\mathcal{L}-1} \subset \cdots \subset W_1 = W_h$. An appropriate spectral problem is defined in the space of W_{i-1} , then the eigenfunctions of the spectral problems are utilized to form W_i . The preconditioner is applied to solve a positive semidefinite linear system which results from discretizing the Darcy flow equation with the lowest order Raviart-Thomas spaces and adopting a trapezoidal quadrature rule. Theoretical analysis and numerical investigations of this preconditioner will be presented. In particular, we will consider several typical highly heterogeneous permeability fields whose resolutions are up to 1024^3 and examine the computational performance of the preconditioner in several aspects, such as strong scalability, weak scalability, and robustness against the contrast of the media. We also demonstrate an application of this preconditioner for solving a two-phase flow benchmark problem.

Keywords: preconditioner, multigrid, Darcy flow, nested multiscale space

2000 MSC: 65N55, 65F08, 65F10

1. Introduction

Simulating fluid flow in porous media is critical for many practical applications, such as reservoir simulation, CO₂ sequestration, nuclear water storage, and underground water contamination. Thanks to the development of reservoir characterization methods, detailed multiscale geocellular models that may contain billions of grid cells become available. Additionally, some simulations, such as CO₂ migration, usually last hundreds of years. As a result, simulating this phenomenon is prohibitively expensive, and it is necessary to perform some model reduction. Generally, there are two categories of model reduction approaches. One is to reduce the model's size by upscaling [1, 2, 3, 4], which is suitable for applications where small details of the flow can be ignored. Another category is multiscale techniques, including the multiscale finite element method [5] and its extensions mixed multiscale finite element method [6, 7], generalized

*Corresponding author.

Email address: sfu@eitech.edu.cn (Shubin Fu)

Preprint submitted to arXiv

March 29, 2024

multiscale finite element method (GMsFEM) [8, 9, 4], multiscale finite volume method [10, 11] and multiscale mortar mixed finite element method [12]. For most of these methods, the basic idea is to solve problems in coarse grids with multiscale basis functions that are constructed by solving carefully defined local problems. These multiscale basis functions are integrated with important information about geological models; hence the accuracy of cheap coarse-grid simulations can be guaranteed.

Although the aforementioned multiscale approaches have been applied successfully to solve a wide range of multiscale problems, multiscale solutions can deteriorate with increasing contrast in permeability and correlation length [13, 14] in certain scenarios. In cases where highly accurate fine-scale solutions are required, it is necessary to design an efficient solver to solve the original fine-scale problems. Direct solvers such as MUMPS [15] are more applicable for problems with multiple sources since these solvers first factorize target operators and then solve linear systems with forward and back substitutions. However, factorizing large-size matrices requires a huge amount of memory, and, worse, the parallel efficiency of direct solvers is not satisfied. Therefore, for large-scale flow simulations which commonly have fixed sources, adopting preconditioned iterative solvers is preferred. Utilizing multiscale coarse spaces is proven to improve the robustness and efficiency of classical preconditioners, and hence, various novel preconditioners [16, 17, 18, 19, 20, 21, 22, 23, 24, 25, 26, 27, 28, 29, 30, 31, 32, 33, 34, 35, 36] have been proposed in past three decades.

Among above mentioned multiscale preconditioners, most of them [16, 17, 18, 19, 20, 21, 22, 23, 24, 25, 26, 27, 28, 29, 30, 35, 37] are developed for handling the elliptic problems in second-order formulation, therefore one can not easily obtain mass conservative velocity fields which limits their applications in flow transport problems. In addition, in these works, local spectral problems are constructed in overlapped subdomains, which implies huge communication that deteriorates the efficiency of parallel computing. In [31, 32, 37], multiscale preconditioners are proposed for solving the saddle system obtained by discretizing the first-order formulation of the elliptic problem, despite their robustness and fast convergence, the degrees of freedom (DoF) of the targeted linear systems are still huge. Moreover, one also needs to solve local spectral problems in overlapped subdomains. To overcome the drawbacks of these multiscale preconditioners, a novel two-grid and two-level multiscale preconditioner is recently developed in [38] and [36] where local spectral problems are defined in non-overlapping coarse blocks. In addition, a velocity elimination technique is adopted to reduce the unknowns of the saddle system without hurting the generation of a mass-conservative velocity field. Although this novel efficient preconditioner shows robustness and impressive computational performance, it is difficult to scale up to extreme-scale problems since solving the coarse problems with direct solvers becomes a bottleneck. A potential remedy is to extend this two-grid/two-level preconditioner to the multi-grid case which is the main goal of this paper. We will construct a sequence of nested spectral subspaces $W_{\mathcal{L}} \subset W_{\mathcal{L}-1} \subset \cdots \subset W_1 = W_h$ and then design a corresponding spectral multigrid preconditioner. The construction of subspace W_i relies on solving spectral problems defined in local W_{i-1} . We note that similar ideas can be found in [39, 35, 33] which also aim to solve the linear system generated by discretizing the second-order formulation of the high-contrast elliptic problem.

Rich numerical experiments will be presented with several typical highly heterogeneous models. In particular, we examine the strong and weak scalability performance and robustness of our preconditioner against contrast ratios of media. Moreover, the implementation of the proposed preconditioner on a two-phase flow benchmark problem is detailed. We want to mention that multiscale preconditioners are not the unique way to cope with high-contrast flow

problems, other types of preconditioners can be found in [40, 41, 42, 43, 44, 45, 46, 14, 47, 48]. Leveraging the convergence theory of inexact two-grid methods, We also provide an analysis of the condition number of the preconditioned operator.

The remainder of the paper is arranged as follows. Section 2 introduces the basic model of subsurface flows, the definition of notation, and fine-scale discretization. Section 3 illustrates a systematic way to construct the coarse space and the preconditioner. An analysis for the proposed preconditioner is presented in Section 4. The numerical results are shown in Section 5. The application of a two-phase flow problem is described in Section 6. Finally, a conclusion is given.

2. Preliminaries

2.1. The model problem and the discretization

We consider the following elliptic PDE with the unknown pressure field p

$$-\operatorname{div}(\mathbb{K}\nabla p) = f \text{ in } \Omega \quad (1)$$

in a bounded Lipschitz domain $\Omega \in \mathbb{R}^d$, with $d = 2$ or 3 , subject to a no-flow boundary condition

$$\mathbb{K}\nabla p \cdot \mathbf{n} = 0 \text{ on } \partial\Omega, \quad (2)$$

where \mathbb{K} is the symmetric matrix-valued permeability field that exhibits discontinuity and high heterogeneity, i.e.,

$$\frac{\max_{\mathbf{x} \in \Omega} \lambda_{\max}(\mathbb{K}(\mathbf{x}))}{\min_{\mathbf{x} \in \Omega} \lambda_{\min}(\mathbb{K}(\mathbf{x}))} \gg 1.$$

In reservoir simulation, the permeability field may not be point-wisely isotropic but commonly be point-wisely orthotropic, that is,

$$\mathbb{K}(\mathbf{x}) = \operatorname{diag}(\kappa^x(\mathbf{x}), \kappa^y(\mathbf{x})) \text{ or } \operatorname{diag}(\kappa^x(\mathbf{x}), \kappa^y(\mathbf{x}), \kappa^z(\mathbf{x})),$$

and we assume the field \mathbb{K} belongs to this class throughout the article. Note that we make a slight abuse of notation for denoting three orthogonal directions by x , y , and z . We emphasize here that the extension of the forthcoming discretization scheme of Eq. (1) to the full matrix-valued permeability field is possible, while several delicate constructions are necessary [49]. The divergence theorem implies that the source function f must satisfy the so-called compatibility condition $\int_{\Omega} f \, d\mathbf{x} = 0$, and an additional restriction $\int_{\Omega} p \, d\mathbf{x} = 0$ must be imposed to guarantee the uniqueness of the solution. However, if we incorporate well modeling (see [50, 51]), the source term f will be coupled with pressure and we will revisit this situation in Section 5. By introducing the flux variable $\mathbf{v} = -\mathbb{K}\nabla p$, we can rewrite Eq. (1) and Eq. (2) as

$$\begin{cases} \mathbb{K}^{-1}\mathbf{v} + \nabla p = \mathbf{0} \text{ in } \Omega, & \text{(Darcy's law),} \\ \operatorname{div}(\mathbf{v}) = f \text{ in } \Omega, & \text{(mass conservation),} \\ \mathbf{v} \cdot \mathbf{n} = 0 \text{ on } \partial\Omega, & \text{(no-flow boundary condition).} \end{cases} \quad (3)$$

Note that for Darcy's law in Eq. (3), we implicitly normalize the viscosity for simplicity.

The mixed formulation (ref. [52]) of Eq. (3) is to seek $(\mathbf{v}, p) \in \mathbf{V} \times W$ satisfying the following equations:

$$\begin{aligned} \int_{\Omega} \mathbb{K}^{-1}\mathbf{v} \cdot \mathbf{w} \, d\mathbf{x} - \int_{\Omega} \operatorname{div}(\mathbf{w})p \, d\mathbf{x} &= 0, & \forall \mathbf{w} \in \mathbf{V}, \\ - \int_{\Omega} \operatorname{div}(\mathbf{v})q \, d\mathbf{x} &= - \int_{\Omega} f q \, d\mathbf{x}, & \forall q \in W. \end{aligned} \quad (4)$$

where the space V is defined as

$$V := \{v \in L^2(\Omega; \mathbb{R}^d) \mid \operatorname{div}(v) \in L^2(\Omega) \text{ and } v \cdot n = 0 \text{ on } \partial\Omega\},$$

and W is

$$W := \left\{ q \in L^2(\Omega) \mid \int_{\Omega} q \, dx = 0 \right\}.$$

By restricting the trial and test functions to finite-dimensional subspaces $V_h \subset V$ and $W_h \subset W$ associated with a prescribed triangulation \mathcal{T}_h of Ω , the corresponding discrete problem is to find $(v_h, p_h) \in V_h \times W_h$ such that

$$\begin{aligned} \int_{\Omega} \mathbb{K}^{-1} v_h \cdot w_h \, dx - \int_{\Omega} \operatorname{div}(w_h) p_h \, dx &= 0, & \forall w_h \in V_h, \\ - \int_{\Omega} \operatorname{div}(v_h) q_h \, dx &= - \int_{\Omega} f q_h \, dx, & \forall q_h \in W_h. \end{aligned} \quad (5)$$

Several well-known families of mixed finite element spaces $V_h \times W_h$ that satisfy the well-known LBB condition can be utilized (see [53]). We choose the lowest-order Raviart-Thomas element space for simplicity, whose definition is detailed in [52, 54]. Let $\{\phi_e\}_{e \in \mathcal{E}_h^0}$ and $\{q_{\tau}\}_{\tau \in \mathcal{T}_h}$ be the bases of V_h and W_h , respectively, where \mathcal{E}_h^0 is the set of internal edges/faces, and we drop h of these bases for brevity. Hence, the finite element solution (v_h, p_h) can be expressed as

$$v_h = \sum_{e \in \mathcal{E}_h^0} v_e \phi_e \text{ and } p_h = \sum_{\tau \in \mathcal{T}_h} p_{\tau} q_{\tau}.$$

Then, it is easy to obtain the following algebraic representation of Eq. (5)

$$\begin{pmatrix} M & -B^{\top} \\ -B & 0 \end{pmatrix} \begin{pmatrix} v \\ p \end{pmatrix} = \begin{pmatrix} 0 \\ -f \end{pmatrix}, \quad (6)$$

where M is a symmetric, positive definite matrix, v , p and f are column vectors.

2.2. The velocity elimination technique

Preconditioning the saddle point system Eq. (6) directly is not easy, and we may involve several sophisticated field-splitting procedures. Fortunately, if applying the trapezoidal quadrature rule to compute the integration $\int_{\Omega} \mathbb{K}^{-1} v_h \cdot w_h \, dx$ on each element, we will obtain a diagonal velocity mass matrix M_t , and hence Eq. (6) could be replaced by

$$\begin{pmatrix} M_t & -B^{\top} \\ -B & 0 \end{pmatrix} \begin{pmatrix} v \\ p \end{pmatrix} = \begin{pmatrix} 0 \\ -f \end{pmatrix}.$$

Since M_t could be inverted straightforwardly and the unknown v in Eq. (6) can be fully eliminated, we boil down to solve a linear system of p as

$$Ap = f, \quad (7)$$

where $A := BM_t^{-1}B^{\top}$ is a symmetric and semi-positive definite matrix. This technique is known as velocity elimination [55, 56, 57], which could also be interpreted as a cell-centered finite

difference scheme on Cartesian meshes. Once \mathbf{p} is solved, the velocity field could be recovered by $\mathbf{v} = \mathbf{M}_t^{-1} \mathbf{B}^T \mathbf{p}$.

Because the analysis result in Section 4 is based on the aforementioned scheme, we elaborate on several details of the discretization here. We limit our discussion to a 2D rectangular domain and structured or Cartesian grids. Let the size of each element be $h^x \times h^y$, the variational form corresponding to the linear system Eq. (7) is

$$\sum_{e \in \mathcal{E}_h^0} \kappa_e \llbracket p_h \rrbracket_e \llbracket q_h \rrbracket_e \frac{|e|^2}{h_x h_y} = \int_{\Omega} f q_h \, d\mathbf{x}, \quad \forall q_h \in W_h, \quad (8)$$

where $|e|$ is the length of the edge e with taking the value of h^x or h^y . The two notations κ_e and $\llbracket \cdot \rrbracket_e$ in Eq. (8) deserve to be addressed: for each internal edge e , $\llbracket p_h \rrbracket_e$ is the jump of p_h across e towards the positive x - or y -direction; the value of κ_e is illustrated in Fig. 1, and the harmonic average stands out as an important property. If we identify f as a function in W_h , the variational form Eq. (8) enjoys an pure algebraic representation as

$$\begin{aligned} \sum_{i,j} \frac{\kappa_{i+1/2,j}}{(h^x)^2} (p_{i+1,j} - p_{i,j}) (q_{i+1,j} - q_{i,j}) \\ + \frac{\kappa_{i,j+1/2}}{(h^y)^2} (p_{i,j+1} - p_{i,j}) (q_{i,j+1} - q_{i,j}) = \sum_{i,j} f_{i,j} q_{i,j}, \end{aligned} \quad (9)$$

and note here we cancel out $h^x h^y$ the area of a fine element on both sides of Eq. (8). The conservation of mass on the fine element could be derived from Eq. (9) as

$$h^y (v_{i+1/2,j} - v_{i-1/2,j}) + h^x (v_{i,j+1/2} - v_{i,j-1/2}) = h^x h^y f_{i,j}$$

with

$$v_{i+1/2,j} = -\kappa_{i+1/2,j} \frac{p_{i+1,j} - p_{i,j}}{h^x} \text{ and } v_{i,j+1/2} = -\kappa_{i,j+1/2} \frac{p_{i,j+1} - p_{i,j}}{h^y}. \quad (10)$$

This scheme shares similarities with finite-volume methods by treating each fine element as a control volume and is termed the two-point flux approximation scheme in the literature [58]. By normalizing \mathbb{K} as

$$\widetilde{\mathbb{K}} = \text{diag}(\widetilde{\kappa}^x, \widetilde{\kappa}^y) := \text{diag}(\kappa^x / (h^x)^2, \kappa^y / (h^y)^2),$$

we can see that

$$\frac{\kappa_{i+1/2,j}}{(h^x)^2} = \widetilde{\kappa}_{i+1/2,j} = \frac{2}{1/\widetilde{\kappa}_{i,j}^x + 1/\widetilde{\kappa}_{i+1,j}^x} \text{ and } \frac{\kappa_{i,j+1/2}}{(h^y)^2} = \widetilde{\kappa}_{i,j+1/2} = \frac{2}{1/\widetilde{\kappa}_{i,j}^y + 1/\widetilde{\kappa}_{i,j+1}^y},$$

which frees Eq. (9) of dimensions of fine elements. This transformation is physically reasonable because the permeability \mathbb{K} is expressed in units of $[\text{Length}]^2$ while $\widetilde{\mathbb{K}}$ is dimensionless. We will utilize this notation in the construction of our preconditioner later.

The main goal of this paper is to develop a spectral multigrid preconditioner for solving Eq. (7).

3. Multiscale coarse space based multigrid preconditioner

To present the construction of coarse spaces, we first explain the decomposition of the domain Ω . We assume that Ω is meshed by \mathcal{L} layers of hierarchical grids that are denoted by $\mathcal{T}^{(l)}$ with

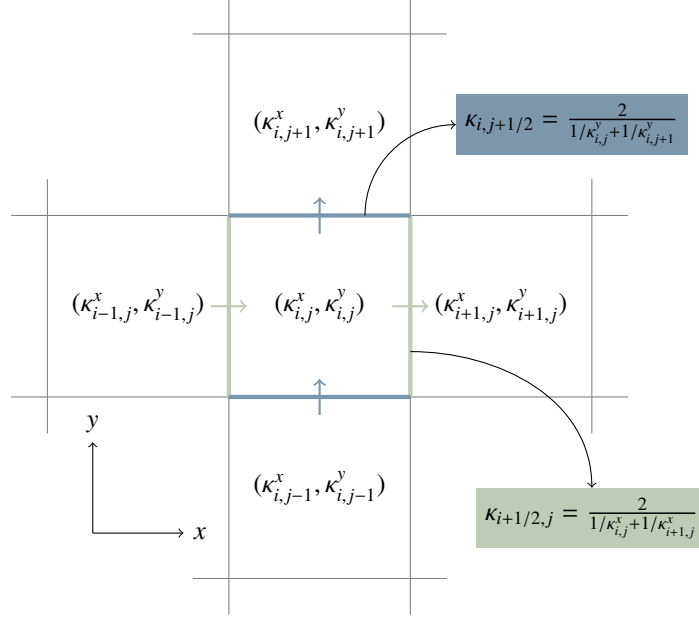


Figure 1: An illustration of the expression of κ_e . Depending on the direction, $\kappa_{i,j+1/2}$ and $\kappa_{i+1/2,j}$ utilize harmonic averages of different component of the permeability field.

$l \in \{0, \dots, \mathcal{L} - 1\}$. The hierarchy implies that each $\mathcal{T}^{(i-1)}$ is a nested refinement of $\mathcal{T}^{(i)}$ for $i = 1, \dots, \mathcal{L} - 1$. Recalling that the finest mesh is $\mathcal{T}_h = \mathcal{T}^{(0)}$ and the resolution of \mathbb{K} is tied to \mathcal{T}_h , We shall treat h as a given physical parameter rather than a variable index in convergence theories of finite element methods.

In this paper, we focus on a three-grid setting, i.e., $\mathcal{L} = 3$. For simplicity of notations, we denote by $\mathcal{T}_c = \mathcal{T}^{(1)}$ the coarse mesh and $\mathcal{T}_{cc} = \mathcal{T}^{(2)}$ the coarse-coarse mesh. This setting is also based on the MPI parallel computing architecture: each MPI process handles a coarse-coarse element in \mathcal{T}_{cc} with ghost layers of the width of one fine element, where ghost layers specialize in inter-process communications; each coarse-coarse element is further partitioned into coarse elements, and there are no inter-process communications required between them. Figure 2 is an illustration of hierarchical meshes, where a fine element τ in \mathcal{T}_h , a coarse element K_c in \mathcal{T}_c , a coarse-coarse element K_{cc} in \mathcal{T}_{cc} and ghost layers are visualized in different colors. We denote by m_c the total number of coarse elements, m_{cc} the total number of coarse-coarse elements, and n the total number of fine elements (also DoF).

A typical three-grid iteration is demonstrated in Algorithm 1. Although, under several assumptions, three-grid or multigrid methods are proven to be convergent (see, e.g., [59, 60]), we, however, exploit them in preconditioned iterative solvers as an acceleration technique (ref. [61]). The matrices M and M_c are the smoothers on the fine and coarse grids, respectively. The two restriction matrices R_c and R_{cc} are crucial ingredients of our preconditioner, and the transposes R_c^T and R_{cc}^T are referred to as prolongation matrices conventionally. Moreover, we have the relations $A_c = R_c A R_c^T$ and $A_{cc} = R_{cc} A R_{cc}^T = (R_{cc} R_c) A (R_{cc} R_c)^T$, where A_{cc} could be singular, and hence the pseudoinverse A_{cc}^\dagger is involved in Algorithm 1. The three-grid method differentiates itself from the two-grid version by the map $r_c \mapsto e_c$ in Algorithm 1, where the latter considers an exact

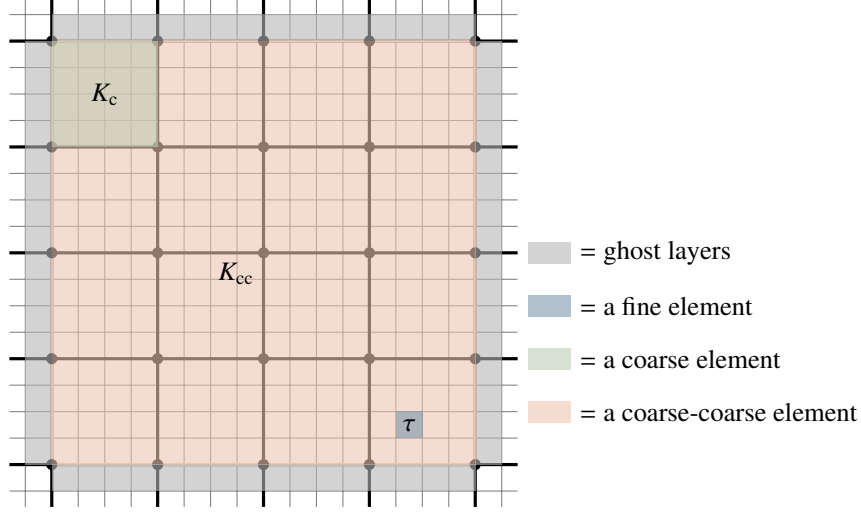


Figure 2: An illustration of hierarchical meshes, a fine element τ , a coarse element K_c , a coarse-coarse element K_{cc} and ghost layers. In MPI-implementations, each K_{cc} is assigned to a unique process.

inversion as $\mathbf{e}_c = \mathbf{A}_c^\dagger \mathbf{r}_c$. In our previous effort [36] on a two-level overlapping preconditioner, we emphasize that the coarse solver is a bottleneck for the computing performance to be scaled up. The aforementioned three-grid method, in some sense, could be viewed as an inexact two-grid method by defining an operator \mathbf{B}_c^{-1} in the following form

$$\begin{aligned} \mathbf{e}_c &= \mathbf{B}_c^{-1} \mathbf{r}_c \\ &:= \left\{ \mathbf{M}_c^{-\top} + \mathbf{M}_c^{-1} - \mathbf{M}_c^{-\top} \mathbf{A}_c \mathbf{M}_c^{-1} + \left(\mathbf{I} - \mathbf{M}_c^{-\top} \mathbf{A}_c \right) \mathbf{R}_{cc}^\top \mathbf{A}_{cc}^\dagger \mathbf{R}_{cc} \left(\mathbf{I} - \mathbf{A}_c \mathbf{M}_c^{-1} \right) \right\} \mathbf{r}_c \end{aligned} \quad (11)$$

as an approximation to \mathbf{A}_c^\dagger .

Algorithm 1 An iteration in three-grid method (preconditioner).

Require: The operators— \mathbf{A} , \mathbf{A}_c , \mathbf{M}^{-1} , \mathbf{M}_c^{-1} , \mathbf{R}_c and \mathbf{R}_{cc} ; the right-hand vector— \mathbf{f} ; an initial guess— $\mathbf{u}^{(0)}$

- | | |
|---|--|
| 1: Presmoothing: $\mathbf{u}^{(1)} \leftarrow \mathbf{u}^{(0)} + \mathbf{M}^{-1}(\mathbf{f} - \mathbf{A}\mathbf{u}^{(0)})$ | ▸ \mathbf{M} is the smoother on the fine grid |
| 2: Restriction: $\mathbf{r}_c \leftarrow \mathbf{R}_c(\mathbf{f} - \mathbf{A}\mathbf{u}^{(1)})$ | ▸ Restrict the residual onto the coarse space |
| 3: Presmoothing: $\mathbf{u}_c^{(0)} \leftarrow \mathbf{M}_c^{-1} \mathbf{r}_c$ | ▸ \mathbf{M}_c is the smoother on the coarse grid |
| 4: Restriction: $\mathbf{r}_{cc} \leftarrow \mathbf{R}_{cc}(\mathbf{r}_c - \mathbf{A}_c \mathbf{u}_c^{(0)})$ | ▸ Restrict the residual onto the coarse-coarse space |
| 5: Correction: $\mathbf{e}_{cc} \leftarrow \mathbf{A}_{cc}^\dagger \mathbf{r}_{cc}$ | ▸ Involve a direct solver on the coarse-coarse grid |
| 6: Prolongation: $\mathbf{u}_c^{(1)} \leftarrow \mathbf{u}_c^{(0)} + \mathbf{R}_{cc}^\top \mathbf{e}_{cc}$ | ▸ Project back into the coarse space |
| 7: Postsmoothing: $\mathbf{e}_c \leftarrow \mathbf{u}_c^{(1)} + \mathbf{M}_c^{-\top}(\mathbf{r}_c - \mathbf{A}_c \mathbf{u}_c^{(1)})$ | ▸ Build the map $\mathbf{r}_c \mapsto \mathbf{e}_c$ |
| 8: Prolongation: $\mathbf{u}^{(2)} \leftarrow \mathbf{u}^{(1)} + \mathbf{R}_c^\top \mathbf{e}_c$ | ▸ Project back into the fine space |
| 9: Postsmoothing: $\mathbf{u}_\star \leftarrow \mathbf{u}^{(2)} + \mathbf{M}^{-\top}(\mathbf{f} - \mathbf{A}\mathbf{u}^{(2)})$ | ▸ The end of the iteration |
-

We then detail the constructions of \mathbf{R}_c and \mathbf{R}_{cc} . For any coarse element $K_c^i \in \mathcal{T}_c$, we define

$W_h(K_c^i)$ by restricting W_h on K_c^i and solve a local spectral problem:

$$\sum_{e \in \mathcal{E}_h^0(K_c^i)} \kappa_e \llbracket \Phi_h \rrbracket_e \llbracket q_h \rrbracket_e \frac{|e|^2}{h_x h_y} = \lambda \int_{K_c^i} (\text{tr } \widetilde{\mathbb{K}}) \Phi_h q_h \, dx, \quad \forall q_h \in W_h(K_c^i), \quad (12)$$

where $\mathcal{E}_h^0(K_c^i)$ is the set of all internal edges in K_c^i , Φ_h is an eigenvector corresponding to the eigenvalue λ and $\widetilde{\mathbb{K}}$ is the normalized permeability field. Note that the eigenvalues here are all dimensionless. Compared to [36], we modify the right-hand bilinear form because the permeability field is now assumed to be orthotropic rather than isotropic. After solving the spectral problem Eq. (12), we construct the local coarse space $W_c(K_c^i)$ as $\text{span}\{\Phi_h^{i,j} \mid j = 0, \dots, l_c^i - 1\}$, where $\{\Phi_h^{i,j}\}_{j=0}^{l_c^i-1}$ are the eigenvectors associated with the smallest eigenvalues L_c^i . By identifying $W_c(K_c^i)$ as a linear subspace of W_h , the global coarse space $W_c \subset W_h$ is formed by $W_c = W_c(K_c^1) \oplus \dots \oplus W_c(K_c^{m_c})$, and n_c —the dimension of W_c —is determined by $n_c = l_c^1 + \dots + l_c^{m_c}$. Therefore, we establish a $\mathbf{R}_c \in \mathbb{R}^{n_c \times n}$ as a restriction matrix from the fine grid to the coarse grid, where each row of it is the algebraic representation of an eigenvector of Eq. (12) in \mathbb{R}^n .

To perform a further dimension reduction on W_c , we propose another spectral problem on each coarse-coarse element $K_{cc}^i \in \mathcal{T}_{cc}$:

$$\sum_{e \in \mathcal{E}_h^0(K_{cc}^i)} \kappa_e \llbracket \Psi_c \rrbracket_e \llbracket \Theta_c \rrbracket_e \frac{|e|^2}{h_x h_y} = \lambda \int_{K_{cc}^i} (\text{tr } \widetilde{\mathbb{K}}) \Psi_c \Theta_c \, dx, \quad \forall \Theta_c \in W_c(K_{cc}^i), \quad (13)$$

where $\mathcal{E}_h^0(K_{cc}^i)$ is the set of all internal edges in K_{cc}^i , $W_c(K_{cc}^i)$ is the restriction of W_c on K_{cc}^i . It should be addressed that Eq. (13) is defined in the linear space $W_c(K_{cc}^i)$ rather than $W_h(K_{cc}^i)$, and this fact may be favorable in two aspects: 1) solving Eq. (13) leads to a smaller algebraic system and should be much easier compared with the latter, and 2) the eigenvectors of Eq. (13) compress the coarse space, while the latter one is irrelevant with W_c . Similarly, the local coarse-coarse space $W_{cc}(K_{cc}^i)$ could be created from spanning $\{\Psi_c^{i,j}\}_{j=0}^{l_{cc}^i-1}$ which are eigenvectors corresponding to the smallest l_{cc}^i eigenvalues. Furthermore, by identifying $W_{cc}(K_{cc}^i)$ as a linear subspace of W_c , we can build the coarse-coarse space W_{cc} as $W_{cc}(K_{cc}^1) \oplus \dots \oplus W_{cc}(K_{cc}^{m_{cc}})$, whose dimension n_{cc} equals $l_{cc}^1 + \dots + l_{cc}^{m_{cc}}$, and thus we achieve a chain of inclusions $W_{cc} \subset W_c \subset W_h$. Back to \mathbf{R}_{cc} , we let each row of $\mathbf{R}_{cc} \mathbf{R}_c$ be the algebraic representation eigenvector Ψ_c of Eq. (13) in \mathbb{R}^n , and \mathbf{R}_{cc} has a shape of $n_{cc} \times n_c$.

Note that the smallest eigenvalue of Eqs. (12) and (13) is always zero and the corresponding eigenfunctions take a constant value. This property implies the kernel space of the left-hand operator in Eq. (8) is contained in W_c and also W_{cc} . Moreover, considering the Raviart-Thomas spaces on \mathcal{T}_c and \mathcal{T}_{cc} , the pressure parts take a constant value on each element, we can hence interpret W_c and W_{cc} as enhancements to classic geometric coarse spaces that are based on nested grids.

Another important fact that could be observed from Eqs. (12) and (13) is that the right-hand operators in algebraic forms are all diagonal matrices. Moreover, if eigenvectors obtained in Eq. (12) are normalized w.r.t. the right-hand bilinear form and are chosen as the bases of W_c , the right-hand operator in the algebraic form of Eq. (13) is an identity matrix, which reduces a generalized eigenvalue problem to a standard one. Those properties are thanks to that the right-hand bilinear forms of Eqs. (12) and (13) are essentially a weighted L^2 inner-product and our coarse elements do not overlap with each other. Constructing coarse spaces via solving spectral

problems is criticized as time-consuming (see [62]), while the proposed spectral problems with a simple right-hand matrix could be expected to alleviate the difficulty.

4. Analysis

To avoid working on singular systems, we suppose that a part of $\partial\Omega$ in Eq. (3) is imposed with a Dirichlet boundary condition, which yields a positive definite matrix \mathbf{A} in Eq. (7). We admit there may exist several subtle modifications for the following theoretical arguments to be applied on a positive semidefinite matrix (cf. [36]). Nevertheless, the numerical experiments that will be presented in the next section support the applicability of the proposed preconditioner on the original problem Eq. (3).

Algorithm 1 determines an inexact two-grid preconditioner \mathbf{P}_{ITG} as

$$\mathbf{P}_{\text{ITG}}^{-1} := \mathbf{M}^{-\top} + \mathbf{M}^{-1} - \mathbf{M}^{-\top} \mathbf{A} \mathbf{M}^{-1} + (\mathbf{I} - \mathbf{M}^{-\top} \mathbf{A}) \mathbf{R}_c^\top \mathbf{B}_c^{-1} \mathbf{R}_c (\mathbf{I} - \mathbf{A} \mathbf{M}^{-1}), \quad (14)$$

where the definition of \mathbf{B}_c^{-1} could be referred to Eq. (11). Accordingly, the exact preconditioner \mathbf{P}_{TG} could be defined as

$$\mathbf{P}_{\text{TG}}^{-1} := \mathbf{M}^{-\top} + \mathbf{M}^{-1} - \mathbf{M}^{-\top} \mathbf{A} \mathbf{M}^{-1} + (\mathbf{I} - \mathbf{M}^{-\top} \mathbf{A}) \mathbf{R}_c^\top \mathbf{A}_c^{-1} \mathbf{R}_c (\mathbf{I} - \mathbf{A} \mathbf{M}^{-1}), \quad (15)$$

and note that \mathbf{B}_c^{-1} in Eq. (14) is replaced by \mathbf{A}_c^{-1} here. Because \mathbf{A} is a positive definite matrix now, we can safely say \mathbf{A}_c and \mathbf{A}_{cc} are invertible. The objective of this section is to provide an upper bound of the condition number of the preconditioned system, that is,

$$\text{cond}(\mathbf{P}_{\text{ITG}}^{-1} \mathbf{A}) := \frac{\lambda_{\max}(\mathbf{P}_{\text{ITG}}^{-1} \mathbf{A})}{\lambda_{\min}(\mathbf{P}_{\text{ITG}}^{-1} \mathbf{A})} \leq C.$$

Since the inexact preconditioner is a perturbation of the exact preconditioner, the results in [59] suggest estimating

$$\text{cond}(\mathbf{P}_{\text{TG}}^{-1} \mathbf{A}) := \frac{\lambda_{\max}(\mathbf{P}_{\text{TG}}^{-1} \mathbf{A})}{\lambda_{\min}(\mathbf{P}_{\text{TG}}^{-1} \mathbf{A})}$$

first.

According to [60], we can see that $\lambda_{\max}(\mathbf{P}_{\text{TG}}^{-1} \mathbf{A}) = 1$. For a positive definite matrix \mathbf{Z} , we take $\|\mathbf{v}\|_{\mathbf{Z}} = \sqrt{\mathbf{v}^\top \mathbf{Z} \mathbf{v}}$ as the energy norm induced by \mathbf{Z} for a compatible vector \mathbf{v} . We usually assume that the smoother \mathbf{M} is properly chosen such that $\mathbf{M} + \mathbf{M}^\top - \mathbf{A}$ is a positive definite matrix. According to [62], a direct result of this assumption is that two-grid iterations can converge without coarse space corrections, although the convergence rate may be poor. Thanks to the XZ-identity [62], we could obtain that

$$\frac{1}{\lambda_{\min}(\mathbf{P}_{\text{TG}}^{-1} \mathbf{A})} = \max_{\mathbf{v} \in \mathbb{R}^n \setminus \{0\}} \min_{\mathbf{v}_c \in \mathbb{R}^{n_c} \setminus \{0\}} \frac{\|\mathbf{v} - \mathbf{R}_c^\top \mathbf{v}_c\|_{\tilde{\mathbf{M}}}^2}{\|\mathbf{v}\|_{\mathbf{A}}^2}, \quad (16)$$

where $\tilde{\mathbf{M}} = \mathbf{M}^\top (\mathbf{M} + \mathbf{M}^\top - \mathbf{A})^{-1} \mathbf{M}$. The special max-min form of Eq. (16) inspires an existence of the optimal coarse space, which is an eigenspace of the generalized eigenvalue problem $\mathbf{A} \mathbf{v} = \lambda \tilde{\mathbf{M}} \mathbf{v}$. Nevertheless, due to the facts that $\tilde{\mathbf{M}}$ requires an inversion of $\mathbf{M} + \mathbf{M}^\top - \mathbf{A}$ and the eigenvalue problem needs to be solved in \mathbb{R}^n , this optimal coarse space is highly unobtainable.

For a coarse element $K_c^i \in \mathcal{T}_c$, we take A_i as the matrix built from the left-hand bilinear form of Eq. (12) and S_i from the right-hand bilinear form, where S_i is a diagonal matrix. We have seen that the coarse grid \mathcal{T}_c consists of non-overlapping coarse elements. It is natural to introduce binary matrices $\{E_1, \dots, E_{m_c}\}$ with the relation $I = E_1^T E_1 + \dots + E_{m_c}^T E_{m_c}$, where the effect of E_i is restricting the DoF of the domain Ω onto the coarse element K_c^i . We have the following relation:

$$\sum_{i=1}^{m_c} E_i^T A_i E_i \lesssim A,$$

where $A' \lesssim A$ means that $A - A'$ is positive semi-definite. This inequality is from taking a summation of the left-hand parts of Eq. (12) w.r.t. all coarse elements, the edges in boundaries of coarse elements will not be counted. Therefore, we can derive that

$$\|v\|_A^2 \geq \sum_{i=1}^{m_c} (E_i v) \cdot A_i (E_i v).$$

To analyses $\|v - R_c^T v\|_{\tilde{M}}$, we inevitably require several assumptions for \tilde{M} . It is known that $A \lesssim \tilde{M}$ via

$$I - A^{1/2} \tilde{M}^{-1} A^{1/2} = (I - A^{1/2} M^{-1} A^{1/2})(I - A^{1/2} M^{-T} A^{1/2}).$$

However, the target here should be bounded \tilde{M} by A . A natural thought is to assume $A \lesssim \tilde{M} \lesssim C_\star A$, which gives exactly an estimate of $\text{cond}(\tilde{M}^{-1} A)$, where $\tilde{M}^{-1} A$ is a preconditioned operator using only the smoother as a preconditioner. Recalling the algebraic representation in Eq. (9), by using a basic inequality, we can show that

$$\begin{aligned} & \sum_{i,j} \tilde{\kappa}_{i+1/2,j} (q_{i+1,j} - q_{i,j})^2 + \tilde{\kappa}_{i,j+1/2} (q_{i,j+1} - q_{i,j})^2 \\ & \leq 2 \sum_{i,j} \tilde{\kappa}_{i+1/2,j} (q_{i+1,j}^2 + q_{i,j}^2) + \tilde{\kappa}_{i,j+1/2} (q_{i,j+1}^2 + q_{i,j}^2) \\ & \leq 2 \sum_{i,j} (\tilde{\kappa}_{i-1/2,j} + \tilde{\kappa}_{i+1/2,j} + \tilde{\kappa}_{i,j-1/2} + \tilde{\kappa}_{i,j+1/2}) q_{i,j}^2, \end{aligned}$$

where boundary cases regarding i and j are omitted for brevity. Thanks to harmonic averages, we can see that

$$\max\{\tilde{\kappa}_{i-1/2,j}, \tilde{\kappa}_{i+1/2,j}, \tilde{\kappa}_{i,j-1/2}, \tilde{\kappa}_{i,j+1/2}\} \leq 2(\tilde{\kappa}_{i,j}^x + \tilde{\kappa}_{i,j}^y).$$

Hence, there exists a generic positive constant C_s such that

$$A \lesssim C_s \sum_{i=1}^{m_c} E_i^T S_i E_i.$$

One may argue that the matrix A here is from discretizing a Dirichlet boundary value problem, while the analysis presented is for the original problem Eq. (3). Based on the velocity elimination technique, the matrix A indeed contains an additional term to the original problem. Fortunately, we can show that this term is a positive diagonal matrix and can also be controlled by $\sum_{i=1}^{m_c} E_i^T S_i E_i$ (ref. [36]). Then, We can derive that

$$\|v - R_c^T v_c\|_{\tilde{M}}^2 \leq C_\star \|v - R_c^T v_c\|_A^2 \leq C_\star C_s \sum_{i=1}^{m_c} (E_i v - E_i R_c^T v_c) \cdot S_i (E_i v - E_i R_c^T v_c).$$

Recalling that each column of \mathbf{R}_c^\top is from solving a generalized eigenvalue problem $\mathbf{A}_i \mathbf{w} = \lambda \mathbf{S}_i \mathbf{w}$ and $\mathbf{E}_i \mathbf{R}_c^\top \mathbf{v}_c$ belongs to the local eigenspace, we can utilize the interpolation property to obtain

$$\min_{\mathbf{v}_c \in \mathbb{R}^{n_c}} \sum_{i=1}^{m_c} (\mathbf{E}_i \mathbf{v} - \mathbf{E}_i \mathbf{R}_c^\top \mathbf{v}_c) \cdot \mathbf{S}_i (\mathbf{E}_i \mathbf{v} - \mathbf{E}_i \mathbf{R}_c^\top \mathbf{v}_c) = \sum_{i=1}^{m_c} \frac{1}{\lambda_{l_c^i}} (\mathbf{E}_i \mathbf{v}) \cdot \mathbf{A}_i (\mathbf{E}_i \mathbf{v}),$$

where $\lambda_{l_c^i}$ is the l_c^i -st smallest¹ eigenvalue. Finally, a lower bound of $\lambda_{\min}(\mathbf{P}_{\text{TG}}^{-1} \mathbf{A})$ can be achieved by controlling the minimal value of $\{\lambda_{l_c^1}, \dots, \lambda_{l_c^{m_c}}\}$.

The estimate of $\text{cond}(\mathbf{P}_{\text{TG}}^{-1} \mathbf{A})$ could be summarized in the following lemma.

Lemma 4.1. *Let C_\star be a positive constant such that $\tilde{\mathbf{M}} \lesssim C_\star \mathbf{A}$, C_λ be $\min\{\lambda_{l_c^i}\}_{i=1}^{m_c}$. Then, the bound*

$$\text{cond}(\mathbf{P}_{\text{TG}}^{-1} \mathbf{A}) \leq \max\left\{C_s \frac{C_\star}{C_\lambda}, 1\right\}$$

holds, where C_s is a generic positive constant.

In [59], Notay provided two-side bounds of the eigenvalues of $\mathbf{P}_{\text{ITG}}^{-1} \mathbf{A}$:

Theorem 4.2. *If $\mathbf{M} + \mathbf{M}^\top - \mathbf{A}$ and \mathbf{A}_c are positive definite matrices. Inequalities*

$$\begin{aligned} \lambda_{\max}(\mathbf{P}_{\text{ITG}}^{-1} \mathbf{A}) &\leq \lambda_{\max}(\mathbf{P}_{\text{TG}}^{-1} \mathbf{A}) \max\{\lambda_{\max}(\mathbf{B}_c^{-1} \mathbf{A}_c), 1\} \text{ and} \\ \lambda_{\min}(\mathbf{P}_{\text{ITG}}^{-1} \mathbf{A}) &\geq \lambda_{\min}(\mathbf{P}_{\text{TG}}^{-1} \mathbf{A}) \min\{\lambda_{\min}(\mathbf{B}_c^{-1} \mathbf{A}_c), 1\} \end{aligned}$$

hold.

Investigating recently developed convergence theories for inexact two-grid preconditioners, e.g. [60, 63], is beyond the scope of the paper. An immediate result of Theorem 4.2 is an estimate of the condition number of $\mathbf{P}_{\text{ITG}}^{-1} \mathbf{A}$ as

$$\text{cond}(\mathbf{P}_{\text{ITG}}^{-1} \mathbf{A}) \leq \text{cond}(\mathbf{P}_{\text{TG}}^{-1} \mathbf{A}) \frac{\max\{\lambda_{\max}(\mathbf{B}_c^{-1} \mathbf{A}_c), 1\}}{\min\{\lambda_{\min}(\mathbf{B}_c^{-1} \mathbf{A}_c), 1\}}.$$

Comparing Eq. (11) with Eq. (15), we realize that \mathbf{B}_c is an exact two-grid preconditioner for \mathbf{A}_c . Hence, two results we mentioned for $\mathbf{P}_{\text{TG}}^{-1} \mathbf{A}$ can also be applied here, i.e.,

$$\lambda_{\max}(\mathbf{B}_c^{-1} \mathbf{A}_c) = 1 \text{ and } \frac{1}{\lambda_{\min}(\mathbf{B}_c^{-1} \mathbf{A}_c)} = \max_{\mathbf{v}_c \in \mathbb{R}^{n_c} \setminus \{0\}} \min_{\mathbf{v}_{cc} \in \mathbb{R}^{n_{cc}} \setminus \{0\}} \frac{\|\mathbf{v}_c - \mathbf{R}_{cc}^\top \mathbf{v}_{cc}\|_{\tilde{\mathbf{M}}_c}^2}{\|\mathbf{v}_c\|_{\mathbf{A}_c}^2},$$

where $\tilde{\mathbf{M}}_c := \mathbf{M}_c^\top (\mathbf{M}_c + \mathbf{M}_c^\top - \mathbf{A}_c)^{-1} \mathbf{M}_c$. Similarly, for a coarse-coarse element $K_{cc}^i \in \mathcal{T}_{cc}$, let $\mathbf{A}_{c,i}$ and $\mathbf{S}_{c,i}$ be two matrices of the bilinear form of the left-hand and right-hand of Eq. (13) by choosing normalized eigenvectors of Eq. (12) as bases. We have mentioned that each $\mathbf{S}_{c,i}$ is exactly an identity matrix. Meanwhile, we can write an algebraic partition of unity on the coarse

¹Using 0-based numbering here.

grid as $\mathbf{I} = \mathbf{E}_{c,1}^\top \mathbf{E}_{c,1} + \cdots + \mathbf{E}_{c,m_{cc}}^\top \mathbf{E}_{c,m_{cc}}$, where each $\mathbf{E}_{c,i}$ is a binary matrix. Based on the same reason for the relation $\sum_{i=1}^{m_c} \mathbf{E}_i^\top \mathbf{A}_i \mathbf{E}_i \lesssim \mathbf{A}$, it can be shown that

$$\sum_{i=1}^{m_{cc}} \mathbf{E}_{c,i}^\top \mathbf{A}_{c,i} \mathbf{E}_{c,i} \lesssim \mathbf{A}_c.$$

Noting that $\widetilde{\mathbf{M}}_c \lesssim \lambda_{\max}(\widetilde{\mathbf{M}}_c) \mathbf{I}$, we have

$$\begin{aligned} \|\mathbf{v}_c - \mathbf{R}_{cc}^\top \mathbf{v}_{cc}\|_{\widetilde{\mathbf{M}}_c}^2 &\leq \lambda_{\max}(\widetilde{\mathbf{M}}_c) \|\mathbf{v}_c - \mathbf{R}_{cc}^\top \mathbf{v}_{cc}\|_1^2 \\ &= \lambda_{\max}(\widetilde{\mathbf{M}}_c) \sum_{i=1}^{m_{cc}} \mathbf{E}_{c,i}(\mathbf{v}_c - \mathbf{R}_{cc}^\top \mathbf{v}_{cc}) \cdot \mathbf{S}_{c,i} \mathbf{E}_{c,i}(\mathbf{v}_c - \mathbf{R}_{cc}^\top \mathbf{v}_{cc}). \end{aligned}$$

Therefore, we can cook up an estimate for $\lambda_{\min}(\mathbf{B}_c^{-1} \mathbf{A}_c)$, which yields the main theorem of this section.

Theorem 4.3. *Let C_\star , C_λ be defined in Lemma 4.1, the constant $C_{c,\lambda}$ be $\min\{\lambda_{i_{cc}}\}_{i=1}^{m_{cc}}$. If $\mathbf{M} + \mathbf{M}^\top - \mathbf{A}$, $\mathbf{M}_c + \mathbf{M}_c^\top - \mathbf{A}_c$, \mathbf{A}_c and \mathbf{A}_{cc} are all positive definite matrices, then*

$$\text{cond}(\mathbf{P}_{\text{ITG}}^{-1} \mathbf{A}) \leq \max \left\{ C_s \frac{C_\star \lambda_{\max}(\widetilde{\mathbf{M}}_c)}{C_\lambda C_{c,\lambda}}, 1 \right\}, \quad (17)$$

where C_s is a generic positive constant.

In Eq. (17), the constants in the numerator are related to the smoothers \mathbf{M} and \mathbf{M}_c , while the constants in the denominator are determined by dimensions of local coarse and coarse-coarse spaces. We admit the current form of Theorem 4.3 is far from completeness. For example, the asymptotic rates of C_λ and $C_{c,\lambda}$ are not depicted. However, our experiments hint that using a modestly large number of eigenvectors is adequate to achieve robustness. Therefore, for Theorem 4.3, we pursue theoretical guidance rather than rigorous analysis.

5. Numerical experiments

In this section, numerical experiments are presented to illustrate the performance of the proposed preconditioner. We consider the unit cube $(0, 1)^3$ as the computational domain Ω with uniformly structured meshes, i.e. $N \times N \times N$ with $h^x = h^y = h^z = 1/N$ for all experiments, and n the total number of DoF also the fine elements is N^3 . We implement the proposed spectral three-grid preconditioner in PETSc [64] and leverage DMDA—a module provided by PETSc—for inter-process communications and data management. As described in Fig. 2, each MPI process owns a coarse-coarse element also a cuboid subdomain, the number of MPI processes hence equals n_{cc} the total number of coarse-coarse elements. Meanwhile, each coarse-coarse element is divided into sd parts in the x -, y - and z -direction, which defines the coarse grid \mathcal{T}_c and determines the relation $n_c = sd^3 \times n_{cc}$. To make the notations more self-explanatory, we take DoF for the number of fine elements (equals n), proc for the number of MPI processes (equals n_{cc}) in the following tables and figures. For the source term f of the model Eq. (3), we place 4 long singular sources at 4 corner points on the $x \times y$ -plane and an opposite sign long singular source at the middle of the $x \times y$ -plane, which mimics the well condition in the SPE10 model (ref. [65]).

For smoother M on A , we will apply ν times block Jacobi iterations, while the block partition is from the coarse grid \mathcal{T}_c . Similarly, for M_c , we will take ν_c times block Jacobi iterations w.r.t. the coarse-coarse grid \mathcal{T}_{cc} . Therefore, we can fix only the 1 ghost layer for all cases, and by contrast, we may use different oversampling layers in overlapping domain decomposition methods (cf. [36]). In the set-up phase, we will perform factorizations for the matrices M , M_c , and A_{cc} . Based on our experience, compared to incomplete Cholesky decompositions, full Cholesky decompositions for M and M_c could decrease iteration numbers but lead to a significant increase in computation time. Therefore, for M and M_c , only incomplete Cholesky factorizations are utilized, while the full LU factorization of A_{cc} is facilitated by an external package SuperLU.DIST [66].

Solving eigenvalue problems is a crucial ingredient in our method, and we employ SLEPc [67]—a companion eigensolver package for PETSc—in the implementation. There are two different strategies in determining dimensions of local coarse and coarse-coarse spaces: (1) use predefined L_c and L_{cc} eigenvectors for all coarse and coarse-coarse elements; (2) set eigenvalue thresholds B_c and B_{cc} , solve enough candidate eigenvectors and then select eigenvectors whose corresponding eigenvalues are below B_c and B_{cc} accordingly. The first approach is relatively easy to implement, while the second is based on Theorem 4.3. The first strategy tends to result in large dimensions of A_c and A_{cc} but balances computing loads among all processes perfectly, while the second is the opposite. We will present a careful comparison of those two strategies later.

We choose the PETSc GMRES method with default parameters to solve the fine system Eq. (6) with a different relative tolerance 10^{-6} , and iteration counts are indicated by `iter`. The HPC cluster in which we run the program is interconnected with an InfiniBand network, and each node is equipped with dual AMD[®] 7452 CPUs (64 CPU cores in total) and 256 GB of memory. We will frequently write the elapsed wall time `time` and iteration count `iter` of an experiment in a format of `time(iter)`, where one effective digit is reserved in the unit of seconds for `time`. Our codes are hosted on GitHub².

5.1. Scalability tests

In this subsection, we fix $(sd, \nu, \nu_c) = (7, 1, 1)$ and adopt the first strategy to construct coarse and coarse-coarse spaces with $(L_c, L_{cc}) = (4, 4)$. A domain Ω consists of periodically duplicated cells, and a cell consists of $8 \times 8 \times 8$ fine elements. Hence, a domain contains $32 \times 32 \times 32$ cells if $\text{DoF} = 256^3$. We set an isotropic \mathbb{K} as $\mathbb{K}(\mathbf{x}) = \kappa(\mathbf{x})I$. The coefficient κ takes values from $\{1, 10^6\}$, and the region of $\kappa(\mathbf{x}) = 10^6$ inside a cell is visualized in Fig. 3a. We demonstrate a domain constructed from $4 \times 4 \times 4$ cells in Fig. 3b, and note that all channels are placed with a high coefficient (10^6) and connected, which is considered as a challenging case for traditional solvers (see [68]). Note that from the setting, the dimension of the square matrix A_{cc} is $\text{proc} \times L_{cc}$, while for A_c it is $\text{proc} \times sd^3 \times L_c$, which is 343 times larger. In our previous work [36], we directly factorized A_c , which accounts for an unsatisfactory scalability performance. We shall witness that the three-grid setting improves scalability significantly.

For strong scalability, we set $\text{DoF} = 512^3$ and choose proc from $\{4^3, 5^3, 6^3, 7^3, 8^3\}$. The results are shown in the left part of Fig. 3c, which contains a graph and a table. A solution process is divided into “Set-up” and “Solve” phases that are colored differently. Recall that “Set-up” contains solving eigenvalue problems and factorizing matrices. Because we only involve a

²<https://github.com/Laphet/PreMixFEM.git>

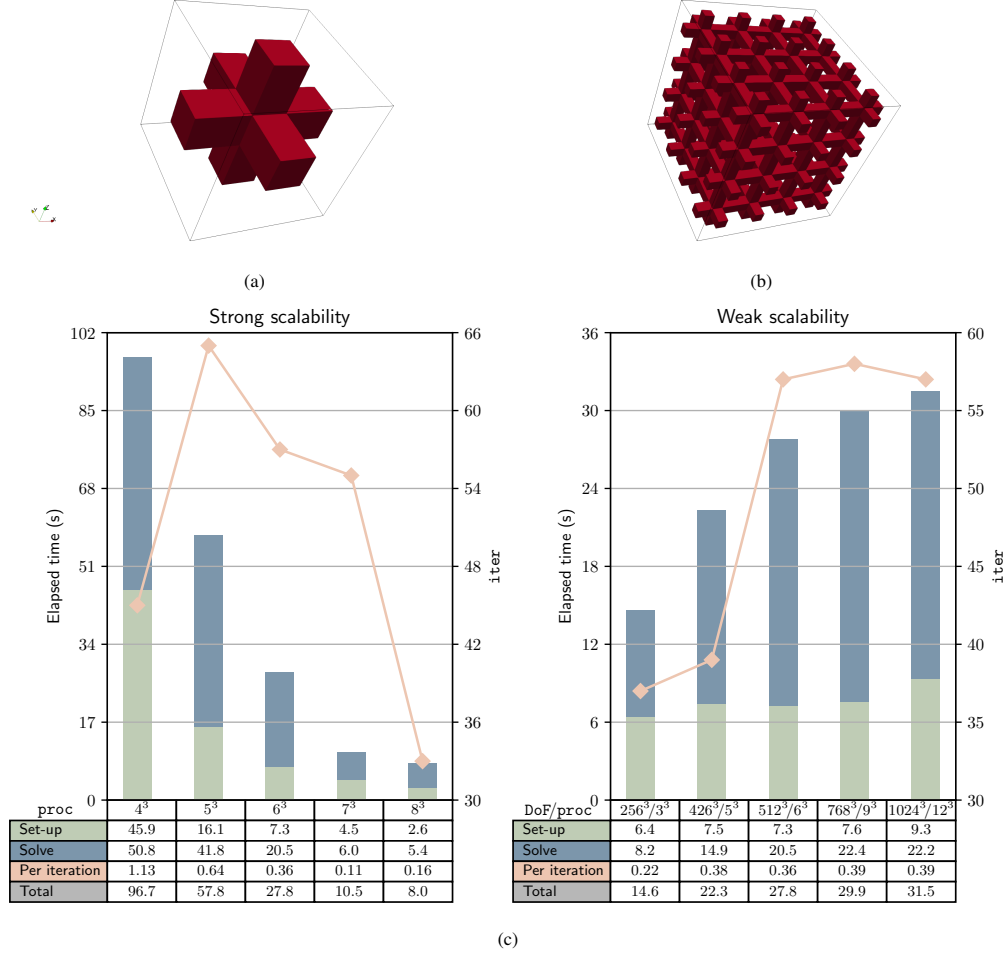


Figure 3: (a) The periodic cell configuration used for the scalability tests. (b) An illustration of a domain that consists of $4 \times 4 \times 4$ cells, where long channels across the domain. (c)-**left** the results of strong scalability tests, where the DoF is fixed as 512^3 and the number of MPI processes varies from $\{4^3, 5^3, 6^3, 7^3, 8^3\}$. (c)-**right** the results of weak scalability tests, where the ratio of DoF and proc is fixed around 85^3 .

direct solver in the LU decomposition of A_{cc} , as expected, the time consumed on “Set-up” for $\text{proc} = 8^3$ is around 6% of $\text{proc} = 4^3$, which is a satisfactory decrease. As a comparison, in our previous work [36], the time consumed on the factorization on the coarse level can increase. We also note that iter does not strictly decrease w.r.t. proc in contrast to what we have observed in [36]. The reason could be that the coarse grid is not aligned with cells, while it is true in [36]. To exclude the influence of different iteration numbers, we calculate the time per iteration in the table. In the “Per iteration” row, we can see that the time decreases by a factor of 10 for proc going from 4^3 to 7^3 but slightly increases for $\text{proc} = 8^3$, and this increase here may be attributed to internode communications.

For weak scalability, we choose DoF from $\{256^3, 426^3, 512^3, 768^3, 1024^3\}$ and proc from

$\{3^3, 5^3, 6^3, 9^3, 12^3\}$ accordingly, while the ratio of DoF and `proc` is fixed around 85^3 . The results are shown in the right part of Fig. 3c. We can see the time consumed on “Set-up” is stable w.r.t. `proc` from 4^3 to 9^3 , and a deterioration of $(9.3/7.6 - 1.0 \approx 12\%)$ is observed for `proc` = 12^3 . From the “Per iteration” row, the time records of `proc` = 5^3 to 12^3 are quite close. We may postulate that the 15% deterioration is due to the direct solver. We could also claim that the current three-grid framework is capable of handling problems of 1 billion DoF or below. However, to extend the proposed method to a larger problem size, truly multigrid and sophisticated load-balancing techniques are crucial. Because there are no inter-node communications needed for `proc` = 3^3 , one may notice that the time, in this case, is considerably less than others.

5.2. Robustness tests on a fractured medium

Modeling flow through fractured porous media is a challenging but important task in reservoir simulation today. Most works treat fractures as planes embedded in the matrix, and the discretization of the domain should be carefully handled (ref. [69]). We here simply discretize the medium with a fine uniform mesh and assign large permeability for fine elements belonging to fractures. In Fig. 4, we demonstrate a fractured medium, where the red and blue regions correspond to the matrix and fractures, respectively. We again set an isotropic \mathbb{K} as $\mathbb{K}(\mathbf{x}) = \kappa(\mathbf{x})\mathbf{I}$, where $\kappa = 1.0$ for matrix and $\kappa = 10^{\text{cf}}$ for fractures. The original resolution of the medium in Fig. 4 is $256 \times 256 \times 256$, and we periodically duplicate it in the domain Ω so that $\text{DoF} = 512^3$.

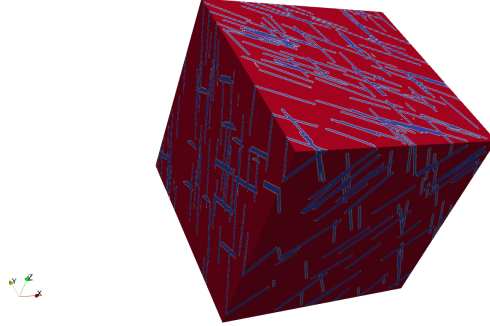


Figure 4: A fractured medium model, where red and blue regions are referred to as matrix (place 1 as the conductivity) and fractures (place 10^{cf} as the conductivity) respectively.

In this subsection, we adopt the first strategy to construct coarse and coarse-coarse spaces and fix $(\text{proc}, \text{sd}, \nu, \nu_c) = (6^3, 7, 1, 1)$. We focus on examining the robustness of the proposed preconditioner w.r.t. contrast ratios and hence choose `cr` from $\{1, 2, 3, 4, 5, 6\}$. As a comparison, performances of two off-the-sheaf preconditioners ASM (Additive Schwarz Method) and GAMG (General Algebraic Multigrid) from PETSc are also recorded. Note that we did not tailor special parameters or options for those preconditioners and just used them in a black-box manner. The results are presented in Table 1, where we fix $L_c = 4$ and choose L_{cc} from $\{4, 8, 11, 17\}$ for the proposed preconditioner. Here the values $\{4, 8, 11, 17\}$ are heuristically determined by the ladder of the eigenvalue sequence

$$\{0, 1, 1, 1, \quad 2, 2, 2, 3, \quad 4, 4, 4, \quad 5, 5, 5, 5, 5, 5, \quad 6, \dots\}$$

Table 1: For the fractured medium model, records of elapsed wall time and iteration numbers of ASM, GAMG, and the proposed preconditioner w.r.t. different contrast ratios, where (*) means the solver does not converge in 1000 iterations and (k^\diamond) means there is a BREAKDOWN error thrown at the step k .

Preconditioner	cr = 1	cr = 2	cr = 3	cr = 4	cr = 5	cr = 6
ASM	135.8(*)	134.5(*)	136.8(*)	135.8(*)	137.1(*)	135.1(*)
GAMG	15.9(14)	19.7(23)	26.8(43)	54.8(117)	45.5(90 $^\diamond$)	46.1(90 $^\diamond$)
$L_c = 4, L_{cc} = 4$	21.9(38)	32.8(70)	40.6(93)	53.9(132)	54.8(137)	55.4(139)
$L_c = 4, L_{cc} = 8$	21.0(31)	26.9(49)	35.1(72)	41.9(89)	49.1(110)	49.7(112)
$L_c = 4, L_{cc} = 11$	20.5(28)	26.6(44)	31.9(60)	38.2(75)	43.2(88)	43.4(89)
$L_c = 4, L_{cc} = 17$	22.6(26)	28.0(39)	31.7(49)	35.3(56)	37.6(62)	37.3(63)

of the Laplace operator.

From Table 1, we can see that ASM performs poorly for this strongly heterogeneous model, and the solver cannot converge in 1000 iterations even for $cr = 1$. As cr increases, the performance of GAMG gradually degrades, i.e., the computation time and iteration numbers all increase. Moreover, we observed BREAKDOWN errors for $cr = 5$ and 6. For the proposed preconditioner, we can notice that it is quite stable w.r.t. contrast ratios. The iteration numbers cannot be completely irrelevant with cr but are well-controlled. Importantly, we did not experience any BREAKDOWN errors in all test cases of the proposed preconditioner. We can also see that including more eigenvectors in the coarse-coarse space greatly stabilizes the performance. For example, the computation time from $cr = 1$ to $cr = 6$ increases only by a factor of 68% for $L_{cc} = 17$, while this number is 152% for $L_{cc} = 4$.

We also carried out several experiments to investigate the influence of L_c on the dimension of local coarse spaces, and the results are shown in Table 2, where $cr = 6$ is set. We can see that a larger L_c could improve the performance, but not significantly compared to L_{cc} . Specifically, if $L_{cc} = 4$, the computation time increases by a factor of 32% from $L_c = 4$ to 17; if $L_c = 4$, the time decreases by a factor of 32% from $L_{cc} = 4$ to 17. Although the minimal iteration number occurs at $(L_c, L_{cc}) = (17, 17)$, the shortest time is found at $(L_c, L_{cc}) = (4, 17)$. The combination effect of L_c and L_{cc} is complicated to be disentangled, while it is advised to enlarge L_{cc} rather than L_c first for improving the final performance.

Table 2: For the fractured medium model, records of elapsed wall time and iteration numbers w.r.t. different L_c and L_{cc} .

L_{cc}	$L_c = 4$	$L_c = 8$	$L_c = 11$	$L_c = 17$
4	55.4(139)	60.0(133)	63.1(129)	72.8(126)
8	49.7(112)	55.3(114)	57.3(110)	67.2(106)
11	44.3(89)	48.3(92)	51.6(90)	60.5(87)
17	37.3(63)	40.6(61)	42.5(59)	50.6(58)

5.3. Tests on the second strategy

It is impossible for SLEPc the eigensolver that we used, to set a target priorly and then find all eigenvectors whose corresponding eigenvalues are below this target. We hence first take a relatively large number into the solver routine, which will produce this number of eigenvectors whose eigenvalues are in ascending order. We can then collect a subset of those eigenvectors and utilize

them to construct the local coarse or coarse-coarse space. According to results in Section 5.2, dimensions of the coarse-coarse space contribute more to the final performance compared with the coarse space. Therefore, we only take the second strategy to construct local coarse-coarse spaces and will fix $L_c = 4$ in the following experiments. On each coarse-coarse element, we compute 20 candidate eigenvectors and select those whose corresponding eigenvalues are below B_{cc} . The construction of the coefficient field follows the same manner as in Section 5.2. For other parameters, we set $(\text{proc}, \text{sd}, \nu, \nu_c) = (6^3, 7, 1, 1)$. The results are presented in Table 3, where the dimensions of the coarse-coarse spaces are also tabulated. In the last row of Table 3, we set $B_{cc} = 10^{12}$ as a reference, which is basically back to the first strategy with $L_{cc} = 20$.

Table 3: Records of elapsed wall time, iteration numbers and dimensions of coarse-coarse spaces w.r.t. different cr and B_{cc} .

B_{cc}	$\text{cr} = 1$	$\text{cr} = 2$	$\text{cr} = 3$	$\text{cr} = 4$	$\text{cr} = 5$	$\text{cr} = 6$
2.0×10^{-4}	23.3(43)	33.4(71)	37.3(73)	40.4(72)	40.4(74)	37.9(75)
	849	895	1748	2125	2381	2381
4.0×10^{-4}	21.1(32)	27.3(47)	32.9(53)	33.5(58)	37.4(62)	38.0(63)
	1491	1723	2742	3169	3222	3222
8.0×10^{-4}	18.9(27)	29.1(39)	30.7(46)	35.5(53)	38.8(60)	39.8(60)
	2679	3438	4109	4218	4220	4221
10^{12}	23.3(24)	29.3(37)	32.6(46)	37.1(53)	39.4(60)	40.4(60)
	4320	4320	4320	4320	4320	4320

We can notice that for $B_c \in \{2.0, 4.0, 8.0\} \times 10^{-4}$, the dimension of the resulting coarse-coarse space increases with cr . It reveals a pattern that eigenvalues of the spectral problem concentrate toward 0 as increasing the contrast ratio, which may explain the necessity of incorporating enough eigenvectors for high contrast problems. But fortunately, the tendency gets saturated as the contrast ratio becomes large, i.e., variances of dimensions for $\text{cr} \in \{4, 5, 6\}$ are noticeably smaller compared with $\text{cr} \in \{1, 2, 3\}$. This observation also explains that the second strategy is more effective for small contrast problems. We can find the following fact to support it: the computation time of $B_{cc} = 8.0 \times 10^{-4}$ at $\text{cr} = 1$ is equal to around 81% of $B_{cc} = 10^{12}$, while this value is 98% at $\text{cr} = 6$. Moreover, we can also conclude that the second strategy exhibits less advantage or even disadvantage over the first strategy for high contrast cases, e.g., the best computation time record in Table 2 is slightly less than Table 3 at $\text{cr} = 6$. To fully leverage the DoF reduction from the second strategy, a load re-balancing procedure should be emphasized and exploited, while it is missed in our current implementation.

5.4. Comparison with the exact preconditioner

We have emphasized repeatedly the defect of the exact two-grid preconditioner, and in this subsection, we will provide several concrete experiments to support the point. We still use the same way in Section 5.2 to produce the permeability field and adopt the first strategy to building local coarse and coarse-coarse spaces. The results are shown in Table 4, where other parameters are set as $(\text{proc}, L_c, L_{cc}, \nu, \nu_c) = (6^3, 4, 8, 1, 1)$. In the last column of Table 4, we also calculate the dimensions of W_c and W_{cc} via $\text{proc} \times \text{sd}^3 \times L_c$ and $\text{proc} \times L_{cc}$.

From Table 4, we can notice that iteration numbers decrease as sd increases in all cases. This phenomenon may be due to the domain decomposition in the implementation that a larger sd means a smaller coarse element, which complies with the convergence theories of traditional

Table 4: Records of elapsed wall time, iteration numbers and dimensions of W_c or W_{cc} of the exact and inexact preconditioner w.r.t. different cr and sd .

sd	Type	cr = 1	cr = 2	cr = 3	cr = 4	cr = 5	cr = 6	Dim
6	exact	32.0(24)	34.6(33)	37.2(42)	39.4(49)	41.2(50)	41.3(50)	186624
	inexact	24.1(32)	31.5(51)	41.7(77)	46.8(91)	53.5(108)	52.3(108)	1728
7	exact	36.9(22)	39.6(29)	45.9(34)	45.4(37)	47.6(37)	48.8(38)	296352
	inexact	21.0(31)	26.9(49)	35.1(72)	41.9(89)	49.1(110)	49.7(112)	1728
8	exact	45.8(20)	48.0(26)	50.4(30)	50.3(32)	57.0(32)	48.5(32)	442368
	inexact	19.7(30)	26.1(46)	37.5(72)	43.6(88)	55.0(110)	53.0(118)	1728

geometric multigrid preconditioners. We can also see that the exact preconditioner is much more robust for contrast ratios than the inexact one. For example, when $sd = 8$ for the exact preconditioner, the iteration number increases by a factor of 60% from $cr = 1$ to $cr = 6$, while this value is 293% for the inexact preconditioner. However, a less iteration number does not always mean better performance. To see this, the records of computation time for the exact preconditioner for $cr = 6$ are longer than the best one in Table 2.

6. Application on two-phase flow problem

In this section, we will apply the proposed preconditioner to solve immiscible and incompressible two-phase (water and oil) flow problems. Physical quantities corresponding to different phases are subscripted as o (oil) and w (water). We assume that the fluid is incompressible, and the governing transportation equation for each phase $\alpha \in \{w, o\}$ is stated as follows:

$$\phi \frac{\partial S_\alpha}{\partial t} + \text{div } \mathbf{v}_\alpha = \widetilde{q}_\alpha, \quad (18)$$

where ϕ is the porosity of the reservoir rock, and for $\alpha \in \{w, o\}$, S_α is the saturation, \mathbf{v}_α is the superficial Darcy velocity that is given by Darcy's law, \widetilde{q}_α is the external sources and sinks but divided by phase's density. Darcy's law for two-phase flows is expressed in the following form:

$$\mathbf{v}_\alpha = -\frac{k_\alpha^r}{\mu_\alpha} \mathbb{K} \nabla p_\alpha. \quad (19)$$

where k_α^r is the relative permeability that depends on the saturation, μ_α is the viscosity, and \mathbb{K} is the orthotropic permeability of the reservoir rock, and p_α is the pressure. Note that gravity is neglected in Eq. (19) for brevity. The fact that the two fluids jointly fill the voids implies the relation

$$S_w + S_o = 1. \quad (20)$$

For simplicity, we also neglect the capillary pressure and hence have

$$p_o - p_w = 0. \quad (21)$$

The system of Eqs. (18) to (21) is overdetermined, and we usually assign p_o and S_w as the two primary variables to cancel out other equations. By defining the total velocity

$$\mathbf{v} = \mathbf{v}_w + \mathbf{v}_o$$

and redefining $p := p_o$, $S := S_w$, Eqs. (18) to (21) are reduced into

$$\mathbf{v} = -\lambda(S)\mathbb{K}\nabla p, \quad (22)$$

$$\text{div } \mathbf{v} = \tilde{q} := \tilde{q}_w + \tilde{q}_o, \quad (23)$$

$$\phi \frac{\partial S}{\partial t} + \text{div}(f_w(S)\mathbf{v}) = \tilde{q}_w, \quad (24)$$

where $\lambda := k_w^r/\mu_w + k_o^r/\mu_o$ is called the total mobility, and $f_w := (k_w^r/\mu_w)/\lambda$ is called the fractional flow function.

The system of Eqs. (22) to (24) is incomplete; for example, the law of k_α^r w.r.t. S_α is missing. We introduce the SPE10 model (ref. [65]) to achieve a thorough description of the problem. The computational domain of the SPE10 model has a physical dimension of $1200 \text{ ft} \times 2200 \text{ ft} \times 170 \text{ ft}$ and contains $60 \times 220 \times 85$ cells, which yields the dimension of fine elements as $(h^x, h^y, h^z) = (20, 10, 2) \text{ ft}$. For the permeability field $\mathbb{K} = \text{diag}(\kappa^x, \kappa^y, \kappa^z)$, κ^x is the same as κ^y and visualized in Fig. 5a, while κ_z is shown in Fig. 5b. We can see that the contrast ratio of κ^x is around 10^8 and the contrast ratio of κ^z is around 10^{11} . We also calculate κ^x/κ^z and present the result in Fig. 5c, which ranges from 1 to 10^4 . The original SPE10 model contains inactive blocks, that is, cells that ϕ take zero. To avoid special treatments for inactive blocks, we modify the original porosity data by truncating ϕ at 0.05, and the modified porosity field is displayed in Fig. 5d.

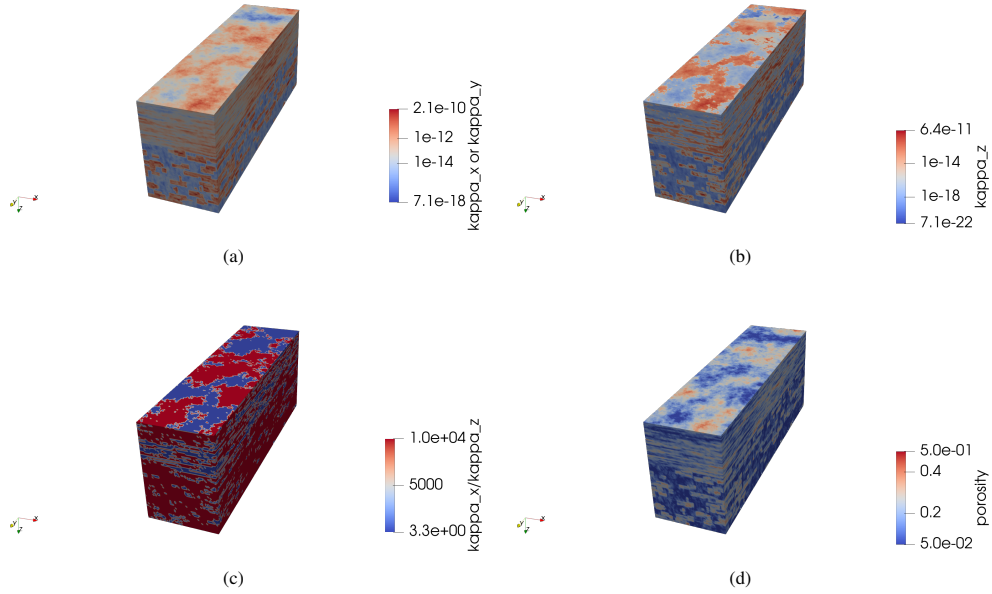


Figure 5: Rock properties of the SPE10 model: (a) κ^x or κ^y , (b) κ^z , (c) κ^x/κ^z , and (d) modified ϕ .

The relative permeabilities k_w^r and k_o^r are given by the following formulas:

$$k_w^r = (S^*)^2, \quad k_o^r = (1 - S^*)^2, \quad S^* = \frac{S - 0.2}{0.6}.$$

The fluid viscosities are taken as $\mu_w = 0.3 \text{ cP}$ and $\mu_o = 3.0 \text{ cP}$. We can hence obtain $\lambda(S)$ and $f_w(S)$ in Eqs. (22) and (24). The no-flow boundary condition is imposed. The source terms \tilde{q}_w

and \tilde{q}_o are determined by well conditions. In the SPE10 model, four production wells are placed in the four corners of the $x \times y$ -plane, and one injection well is located in the center of the $x \times y$ -plane. All wells are vertical and penetrate completely throughout the domain. For the central injector, the injection rate is fixed as 5000 bbl/day. Therefore, for all cells that contact the central injector, we set the same \tilde{q}_w such that the summation equals the prescribed injection rate. For four producers, only the bottom hole pressure $p_{BH} = 4000$ psi is provided. For a cell that contacts a producer, the local pressure p_α and source \tilde{q}_α satisfy

$$\text{WI} \frac{\kappa}{\mu_\alpha} (p_{BH} - p_\alpha) = \tilde{q}_\alpha,$$

where WI is called the well index, κ is the local κ^x or κ^y . Following the instruction in [50], we engineered the well index as

$$\text{WI} = \frac{\frac{1}{(h^x)^2} + \frac{1}{(h^y)^2}}{\frac{2}{\pi} \left(\frac{h^y}{h^x} \log \frac{r_1}{r_{wb}} + \frac{h^x}{h^y} \log \frac{r_2}{r_{wb}} \right) - 1},$$

where $r_1 = \sqrt{9(h^x)^2 + (h^y)^2}/2$, $r_2 = \sqrt{(h^x)^2 + 9(h^y)^2}/2$, r_{wb} is termed the wellbore radius and takes the value 1.0 ft. Note now the right-hand term of Eq. (23) is coupled with p , which differs from the original problem Eq. (3). The initial condition in the SPE10 model is $S = 0.2$, i.e., the initial water saturation equals 0.2 in all cells.

We adopt the improved implicit pressure and explicit saturation (IMPES) method (ref. [70, 71, 50]) to solve this coupled system Eqs. (22) to (24). More specifically, assuming that at the n -th time step, the saturation S^n is known, we solve the system

$$\begin{cases} \mathbf{v}^{n+1} = -\lambda(S^n) \mathbb{K} \nabla p^{n+1}, \\ \text{div } \mathbf{v}^{n+1} = \tilde{q}(p^{n+1}), \end{cases} \quad (25)$$

via the discretization scheme from the velocity elimination technique to obtain the updated p^{n+1} and \mathbf{v}^{n+1} . Then, set $S^{n,0} := S^n$, for any fine element τ , update the local saturation $(S^{n,m}|_\tau \rightarrow S^{n,m+1}|_\tau)$ by the explicit Euler time discretization of Eq. (24) as

$$\phi|_\tau \frac{S^{n,m+1}|_\tau - S^{n,m}|_\tau}{\delta t^{n,m}} + \frac{1}{|\tau|} \int_{\partial\tau} f_w(S^{n,m}) \mathbf{v}^{n+1} \cdot \mathbf{n} \, dA = \tilde{q}_w(p^{n+1}|_\tau), \quad (26)$$

where $\delta t^{n,m}$ is chosen adaptively such that the maximal variance of $S^{n,m+1}$ and $S^{n,m}$ will not exceed DS_{\max} , and $f_w(S^{n,m})|_{\partial\tau}$ should be determined by the upstream weighting rule (see [50]). After M iterations, an updated saturation field is obtained by $S^{n+1} = S^{n,M}$. As a comparison, in the classic IMPES method, the routine Eq. (26) is performed only once. We realize that Eq. (26) could be fully parallelized while solving Eq. (25) dominates the overall computation time.

We employ the proposed spectral preconditioner in solving Eq. (25) and set the relative tolerance at 10^{-9} . To accommodate the well condition, we modify the left-hand bilinear forms in Eqs. (12) and (13) accordingly. Except for p^0 the first step of pressure, solving Eq. (25) could significantly benefit from considering the previous p^n as the initial guess for iterative solvers. Noting that the DoF of the SPE10 model equals to $60 \times 220 \times 85$, we hence set $\text{proc} = 2 \times 7 \times 3$ to equally distribute subdomains and also avoid inter-node communications. We adopt the first strategy in constructing local coarse and coarse-coarse spaces and fix $\text{sd} = 4$. The rest parameters in the improved IMPES are chosen as $(\text{DS}_{\max}, M) = (0.001, 50)$. The performance is also

benchmarked against the default algebraic multigrid preconditioner (GAMG) of PETSc. In the first group of experiments, we aim to investigate different choices of (L_c, L_{cc}) from $\{4, 8\} \times \{4, 8\}$ with $(\nu, \nu_c) = (1, 1)$, and the computation time and iteration number of each updating pressure step (that is, solving Eq. (25)) are shown in Figs. 6a and 6b. In the second group of experiments, we set different numbers of block Jacobi iterations within the smoothers while fixing (L_c, L_{cc}) , that is, we take $(\nu, \nu_c) \in \{1, 2\} \times \{1, 2\}$ with $(L_c, L_{cc}) = (4, 8)$, and the results are presented in Figs. 6c and 6d. Because there is no proper initial guess available for solving p^0 , the computing records regarding the first updating pressure step are outliers compared to other steps, and we hence exclude them in Figs. 6a to 6d.

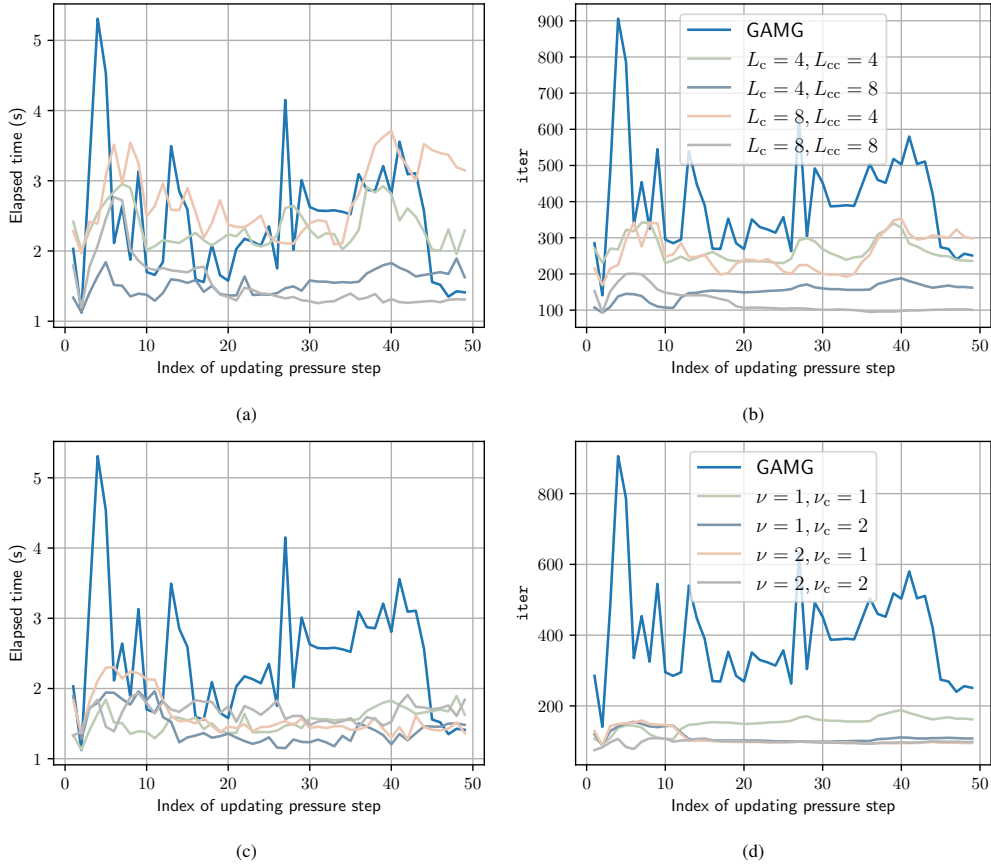


Figure 6: The elapsed time and iteration numbers of the first 50 updating pressure steps. (a) and (b) share the same setting that $(\nu, \nu_c) = (1, 1)$ but (L_c, L_{cc}) from $\{4, 8\} \times \{4, 8\}$. (c) and (d) share the same setting that $(L_c, L_{cc}) = (4, 8)$ but $(\nu, \nu_c) \in \{1, 2\} \times \{1, 2\}$.

The first impression from Fig. 6 could be that GAMG exhibits larger variances in terms of elapsed time and iteration numbers; that is, GAMG performs less robustly compared to the proposed preconditioner. From Figs. 6a and 6b, we can see that larger L_c and L_{cc} can help to stabilize the performance, and it seems that the setting $(L_c, L_{cc}) = (4, 8)$ slightly outperforms than others regarding stability and efficiency. According to Figs. 6c and 6d, the effect of different ν

and ν_c is rather weak, while the setting $(\nu, \nu_c) = (1, 2)$ surpasses by a narrow margin.

The original SPE10 project requires simulating 2000 days of production. We are also capable of performing the 2000-day simulation with the proposed preconditioner. The saturation of the water over several time frames is visualized in Fig. 7. We can observe that the water saturation is much higher around the injector and that the oil is driven by water to the producers. The improved IMPES loosens the restrictions on time-step sizes, but they are not large enough for the 2000-day simulation. We note with the help of [72], we are able to apply our method for more realistic models such as Watt field [73], which is based on a combination of synthetic data and real data from a North Sea oil field. Fig. 8 show the permeability of the Watt model and saturation profiles at different time. Currently, full implicit time methods with Constrained Pressure Residual (CPR) preconditioners (see [74, 75]) are preferred by industry solvers. A computing hotspot in CPR is inexact solving the pressure equation, which the proposed preconditioner could be naturally integrated into.

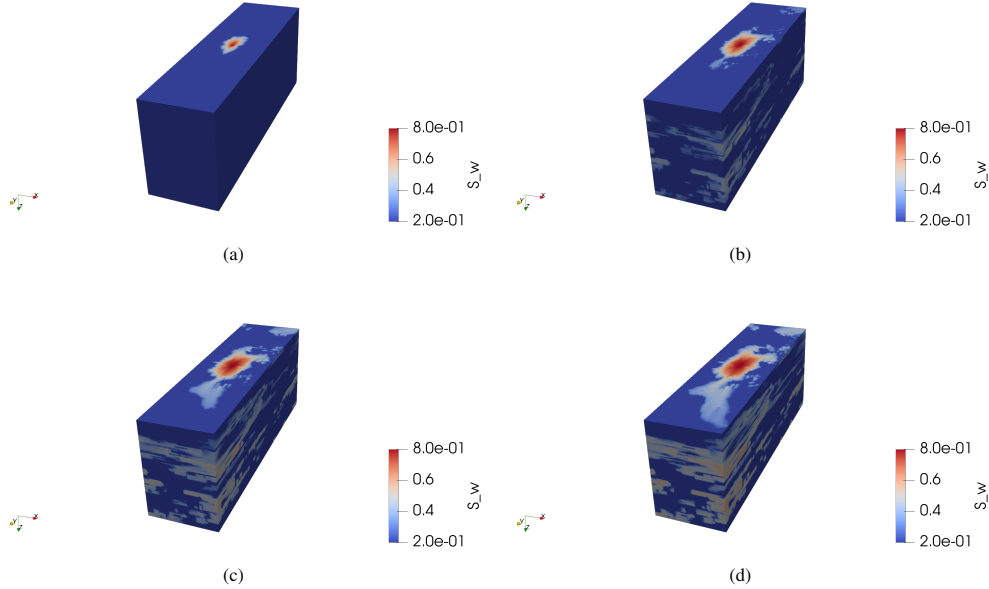


Figure 7: The water saturation of the SPE10 model at different time: (a) $t = 60.17$ days, (b) $t = 520.04$ days, (c) $t = 1211.85$ days, (d) $t = 1995.13$ days.

7. Conclusion

In this paper, we developed a spectral multigrid preconditioner for Darcy flow in high-contrast media. The core component of this preconditioner is to incorporate a sequence of nested multiscale subspaces which is crucial for improving the robustness of the preconditioner. These subspaces can be constructed recursively by solving carefully designed local spectral problems. The condition number of this preconditioner is estimated and rich typical numerical examples

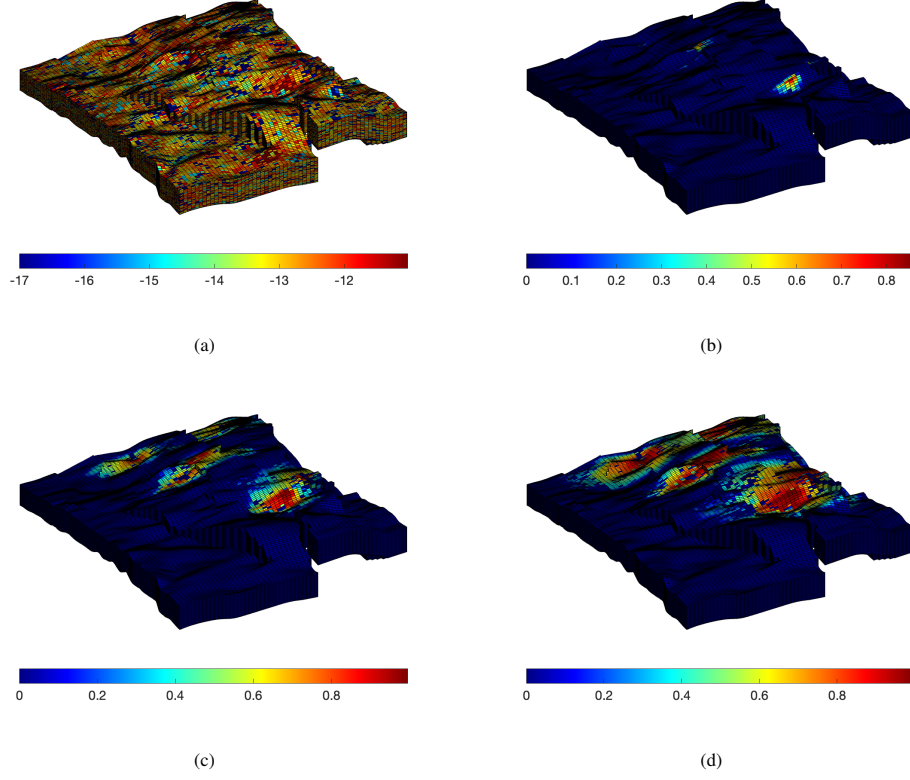


Figure 8: (a) Permeability field of the Watt field model. (b)-(d) The water saturation of the Watt field model at different time: (b) $t = 243.50$ days, (c) $t = 5113.40$ days, (d) $t = 29462.90$ days.

are provided to exhibit the robustness and scalability of the algorithm. Applications for incompressible two-phase flow problems are presented. We plan to study this preconditioner for more complicated underground flow problems such as block oil simulations.

Acknowledgements

JH's research is supported by National Key Research and Development Project of China (No. 2023YFA1011705) and National Natural Science Foundation of China (Project numbers: 12131002). SF's research is supported by startup funding of Eastern institute of technology, Ningbo, NSFC (Project number: 12301514) and Ningbo Yongjiang Talent Programme. SF would like to thank Dr. Olav Møyner for providing dataset of Watt model. Research of EC is partially supported by the Hong Kong RGC General Research Fund (Project numbers: 14305222 and 14304021).

References

- [1] X. H. Wu, Y. Efendiev, T. Y. Hou, Analysis of upscaling absolute permeability, *Discrete and Continuous Dynamical Systems. Series B. A Journal Bridging Mathematics and Sciences* 2 (2) (2002) 185–204. doi:10.3934/dcdsb.2002.2.185.
- [2] L. J. Durlofsky, Numerical calculation of equivalent grid block permeability tensors for heterogeneous porous media, *Water Resources Research* 27 (5) (1991) 699–708. doi:10.1029/91WR00107.
- [3] T. Arbogast, H. Xiao, A multiscale mortar mixed space based on homogenization for heterogeneous elliptic problems, *SIAM Journal on Numerical Analysis* 51 (1) (2013) 377–399. doi:10.1137/120874928.
- [4] E. Chung, Y. Efendiev, T. Y. Hou, *Multiscale model reduction*, Springer Cham, 2023. doi:10.1007/978-3-031-20409-8.
- [5] T. Y. Hou, X.-H. Wu, A multiscale finite element method for elliptic problems in composite materials and porous media, *Journal of Computational Physics* 134 (1) (1997) 169–189. doi:10.1006/jcph.1997.5682.
- [6] Z. Chen, T. Y. Hou, A mixed multiscale finite element method for elliptic problems with oscillating coefficients, *Mathematics of Computation* 72 (242) (2003) 541–576. doi:10.1090/S0025-5718-02-01441-2.
- [7] J. r. E. Aarnes, On the use of a mixed multiscale finite element method for greater flexibility and increased speed or improved accuracy in reservoir simulation, *Multiscale Modeling & Simulation. A SIAM Interdisciplinary Journal* 2 (3) (2004) 421–439. doi:10.1137/030600655.
- [8] Y. Efendiev, J. Galvis, T. Y. Hou, Generalized multiscale finite element methods (GMsFEM), *Journal of Computational Physics* 251 (2013) 116–135. doi:10.1016/j.jcp.2013.04.045.
- [9] E. T. Chung, Y. Efendiev, C. S. Lee, Mixed generalized multiscale finite element methods and applications, *Multiscale Modeling & Simulation. A SIAM Interdisciplinary Journal* 13 (1) (2015) 338–366. doi:10.1137/140970574.
- [10] P. Jenny, S. H. Lee, H. A. Tchelepi, Multi-scale finite-volume method for elliptic problems in subsurface flow simulation, *Journal of Computational Physics* 187 (1) (2003) 47–67. doi:10.1016/S0021-9991(03)00075-5.
- [11] H. Hajibeygi, P. Jenny, Multiscale finite-volume method for parabolic problems arising from compressible multiphase flow in porous media, *Journal of Computational Physics* 228 (14) (2009) 5129–5147. doi:10.1016/j.jcp.2009.04.017.
- [12] T. Arbogast, G. Pencheva, M. F. Wheeler, I. Yotov, A multiscale mortar mixed finite element method, *Multiscale Modeling & Simulation. A SIAM Interdisciplinary Journal* 6 (1) (2007) 319–346. doi:10.1137/060662587.
- [13] I. Lunati, P. Jenny, Treating highly anisotropic subsurface flow with the multiscale finite-volume method, *Multiscale Modeling & Simulation. A SIAM Interdisciplinary Journal* 6 (1) (2007) 308–318. doi:10.1137/050638928.
- [14] T. Arbogast, H. Xiao, Two-level mortar domain decomposition preconditioners for heterogeneous elliptic problems, *Computer Methods in Applied Mechanics and Engineering* 292 (2015) 221–242, special Issue on Advances in Simulations of Subsurface Flow and Transport (Honoring Professor Mary F. Wheeler). doi:10.1016/j.cma.2014.10.049.
- [15] P. R. Amestoy, I. S. Duff, J.-Y. L'Excellent, J. Koster, A fully asynchronous multifrontal solver using distributed dynamic scheduling, *SIAM Journal on Matrix Analysis and Applications* 23 (1) (2001) 15–41. doi:10.1137/s0895479899358194.
- [16] I. G. Graham, R. Scheichl, Robust domain decomposition algorithms for multiscale PDEs, *Numerical Methods for Partial Differential Equations. An International Journal* 23 (4) (2007) 859–878. doi:10.1002/num.20254.
- [17] M. Sarkis, Nonstandard coarse spaces and Schwarz methods for elliptic problems with discontinuous coefficients using non-conforming elements, *Numerische Mathematik* 77 (3) (1997) 383–406. doi:10.1007/s002110050292.
- [18] P. E. Bjørstad, P. Krzyżanowski, A flexible 2-level Neumann-Neumann method for structural analysis problems, in: R. Wyrzykowski, J. Dongarra, M. Paprzycki, J. Waśniewski (Eds.), *Parallel Processing and Applied Mathematics*, Springer Berlin Heidelberg, Berlin, Heidelberg, 2002, pp. 387–394.
- [19] Y. Wang, H. Hajibeygi, H. A. Tchelepi, Algebraic multiscale solver for flow in heterogeneous porous media, *Journal of Computational Physics* 259 (2014) 284–303. doi:10.1016/j.jcp.2013.11.024.
- [20] J. G. Calvo, O. B. Widlund, An adaptive choice of primal constraints for BDDC domain decomposition algorithms, *Electronic Transactions on Numerical Analysis* 45 (2016) 524–544.
- [21] H. H. Kim, E. Chung, J. Wang, BDDC and FETI-DP preconditioners with adaptive coarse spaces for three-dimensional elliptic problems with oscillatory and high contrast coefficients, *Journal of Computational Physics* 349 (2017) 191–214. doi:10.1016/j.jcp.2017.08.003.
- [22] V. Dolean, F. Nataf, R. Scheichl, N. Spillane, Analysis of a two-level Schwarz method with coarse spaces based on local Dirichlet-to-Neumann maps, *Computational Methods in Applied Mathematics* 12 (4) (2012) 391–414. doi:10.2478/cmam-2012-0027.
- [23] H. H. Kim, E. Chung, J. Wang, BDDC and FETI-DP algorithms with a change of basis formulation on adap-

- tive primal constraints, *Electronic Transactions on Numerical Analysis* 49 (2018) 64–80. doi:10.1553/etna_vol149s64.
- [24] A. Klawonn, P. Radtke, O. Rheinbach, FETI-DP methods with an adaptive coarse space, *SIAM Journal on Numerical Analysis* 53 (1) (2015) 297–320. doi:10.1137/130939675.
 - [25] J. Mandel, B. Sousedik, Adaptive selection of face coarse degrees of freedom in the BDDC and the FETI-DP iterative substructuring methods, *Computer Methods in Applied Mechanics and Engineering* 196 (8) (2007) 1389–1399. doi:10.1016/j.cma.2006.03.010.
 - [26] J. Galvis, Y. Efendiev, Domain decomposition preconditioners for multiscale flows in high-contrast media, *Multiscale Modeling & Simulation. A SIAM Interdisciplinary Journal* 8 (4) (2010) 1461–1483. doi:10.1137/090751190.
 - [27] J. Galvis, Y. Efendiev, Domain decomposition preconditioners for multiscale flows in high contrast media: reduced dimension coarse spaces, *Multiscale Modeling & Simulation. A SIAM Interdisciplinary Journal* 8 (5) (2010) 1621–1644. doi:10.1137/100790112.
 - [28] F. Nataf, H. Xiang, V. Dolean, N. Spillane, A coarse space construction based on local Dirichlet-to-Neumann maps, *SIAM Journal on Scientific Computing* 33 (4) (2011) 1623–1642. doi:10.1137/100796376.
 - [29] A. Klawonn, P. Radtke, O. Rheinbach, A comparison of adaptive coarse spaces for iterative substructuring in two dimensions, *Electronic Transactions on Numerical Analysis* 45 (2016) 75–106.
 - [30] A. Heinlein, A. Klawonn, J. Knepper, O. Rheinbach, Adaptive GDSW coarse spaces for overlapping Schwarz methods in three dimensions, *SIAM Journal on Scientific Computing* 41 (5) (2019) A3045–A3072. doi:10.1137/18M1220613.
 - [31] H. Xie, X. Xu, Domain decomposition preconditioners for mixed finite-element discretization of high-contrast elliptic problems, *Communications on Applied Mathematics and Computation* 1 (1) (2019) 141–165. doi:10.1007/s42967-019-0005-z.
 - [32] Y. Yang, S. Fu, E. T. Chung, A two-grid preconditioner with an adaptive coarse space for flow simulations in highly heterogeneous media, *Journal of Computational Physics* 391 (2019) 1–13. doi:10.1016/j.jcp.2019.03.038.
 - [33] H. Al Daas, L. Grigori, P. Jolivet, P.-H. Tournier, A multilevel Schwarz preconditioner based on a hierarchy of robust coarse spaces, *SIAM Journal on Scientific Computing* 43 (3) (2021) A1907–A1928. doi:10.1137/19M1266964.
 - [34] H. Xie, X. Xu, Mass conservative domain decomposition preconditioners for multiscale finite volume method, *Multiscale Modeling & Simulation. A SIAM Interdisciplinary Journal* 12 (4) (2014) 1667–1690. doi:10.1137/130936555.
 - [35] P. Bastian, R. Scheichl, L. Seelinger, A. Strehlow, Multilevel spectral domain decomposition, *SIAM Journal on Scientific Computing* (2022) S1–S26 doi:10.1137/21m1427231.
 - [36] C. Ye, S. Fu, E. T. Chung, J. Huang, A robust two-level overlapping preconditioner for Darcy flow in high-contrast media, (submitted to *SIAM Journal on Scientific Computing*) (Mar. 2023).
 - [37] D. Z. Kalchev, C. S. Lee, U. Villa, Y. Efendiev, P. S. Vassilevski, Upscaling of mixed finite element discretization problems by the spectral AMGe method, *SIAM Journal on Scientific Computing* 38 (5) (2016) A2912–A2933. doi:10.1137/15M1036683.
 - [38] S. Fu, E. Chung, I. Zhao, An efficient multiscale preconditioner for large-scale highly heterogeneous flow, (To appear in *SIAM Journal on Scientific Computing*) (2022).
 - [39] Y. Efendiev, J. Galvis, P. S. Vassilevski, Spectral element agglomerate algebraic multigrid methods for elliptic problems with high-contrast coefficients, in: *Domain decomposition methods in science and engineering XIX*, Vol. 78 of *Lect. Notes Comput. Sci. Eng.*, Springer, Heidelberg, 2011, pp. 407–414. doi:10.1007/10.1007/978-3-642-11304-8_47.
 - [40] H. Yang, S. Sun, Y. Li, C. Yang, A fully implicit constraint-preserving simulator for the black oil model of petroleum reservoirs, *Journal of Computational Physics* 396 (2019) 347–363. doi:10.1016/j.jcp.2019.05.038.
 - [41] N. Yang, H. Yang, C. Yang, Multilevel field-split preconditioners with domain decomposition for steady and unsteady flow problems, *Computer Physics Communications* 280 (2022) 108496. doi:10.1016/j.cpc.2022.108496.
 - [42] R. Li, H. Yang, C. Yang, Parallel multilevel restricted Schwarz preconditioners for implicit simulation of subsurface flows with Peng-Robinson equation of state, *Journal of Computational Physics* 422 (2020) 109745. doi:10.1016/j.jcp.2020.109745.
 - [43] H. Yang, Z. Zhu, J. Kou, A minimum-type nonlinear complementarity simulator with constrained pressure residual (CPR) methods for wormhole propagation in carbonate acidization, *Journal of Computational Physics* 473 (2023) 111732. doi:10.1016/j.jcp.2022.111732.
 - [44] L. Luo, X.-C. Cai, D. E. Keyes, Nonlinear preconditioning strategies for two-phase flows in porous media discretized by a fully implicit discontinuous Galerkin method, *SIAM Journal on Scientific Computing* 43 (5) (2021) S317–S344. doi:10.1137/20m1344652.

- [45] X. Hu, S. Wu, X.-H. Wu, J. Xu, C.-S. Zhang, S. Zhang, L. Zikatanov, Combined preconditioning with applications in reservoir simulation, *Multiscale Modeling & Simulation. A SIAM Interdisciplinary Journal* 11 (2) (2013) 507–521. doi:10.1137/120885188.
- [46] X. Hu, J. Xu, C. Zhang, Application of auxiliary space preconditioning in field-scale reservoir simulation, *Science China. Mathematics* 56 (12) (2013) 2737–2751. doi:10.1007/s11425-013-4737-3.
- [47] B. Ganis, K. Kumar, G. Pencheva, M. F. Wheeler, I. Yotov, A multiscale mortar method and two-stage preconditioner for multiphase flow using a global Jacobian approach, in: *SPE Large Scale Computing and Big Data Challenges in Reservoir Simulation Conference and Exhibition*, Vol. All Days, 2014, SPE-172990-MS. doi:10.2118/172990-MS.
- [48] B. Ganis, G. Pencheva, M. F. Wheeler, T. Wildey, I. Yotov, A frozen Jacobian multiscale mortar preconditioner for nonlinear interface operators, *Multiscale Modeling & Simulation. A SIAM Interdisciplinary Journal* 10 (3) (2012) 853–873. doi:10.1137/110826643.
- [49] R. Ingram, M. F. Wheeler, I. Yotov, A multipoint flux mixed finite element method on hexahedra, *SIAM Journal on Numerical Analysis* 48 (4) (2010) 1281–1312. doi:10.1137/090766176.
- [50] Z. Chen, *Reservoir simulation*, Vol. 77 of CBMS-NSF Regional Conference Series in Applied Mathematics, Society for Industrial and Applied Mathematics (SIAM), Philadelphia, PA, 2007, mathematical techniques in oil recovery. doi:10.1137/1.9780898717075.
- [51] Z. Chen, G. Huan, Y. Ma, *Computational methods for multiphase flows in porous media*, Vol. 2 of Computational Science & Engineering, Society for Industrial and Applied Mathematics (SIAM), Philadelphia, PA, 2006. doi:10.1137/1.9780898718942.
- [52] F. Brezzi, M. Fortin, *Mixed and hybrid finite element methods*, Vol. 15 of Springer Series in Computational Mathematics, Springer-Verlag, New York, 1991. doi:10.1007/978-1-4612-3172-1.
- [53] F. Auricchio, L. Beirão da Veiga, F. Brezzi, C. Lovadina, *Mixed finite element methods*, John Wiley & Sons, Ltd, 2017, pp. 1–53. doi:10.1002/9781119176817.ecm2004.
- [54] D. Boffi, F. Brezzi, M. Fortin, *Mixed finite element methods and applications*, Vol. 44 of Springer Series in Computational Mathematics, Springer, Heidelberg, 2013. doi:10.1007/978-3-642-36519-5.
- [55] T. F. Russell, M. F. Wheeler, *Finite element and finite difference methods for continuous flows in porous media*, Society for Industrial and Applied Mathematics (SIAM), Philadelphia, PA, 1983, Ch. 2, pp. 35–106. doi:10.1137/1.9781611971071.ch2.
- [56] T. Arbogast, M. F. Wheeler, I. Yotov, Mixed finite elements for elliptic problems with tensor coefficients as cell-centered finite differences, *SIAM Journal on Numerical Analysis* 34 (2) (1997) 828–852. doi:10.1137/S0036142994262585.
- [57] J. Chen, E. T. Chung, Z. He, S. Sun, Generalized multiscale approximation of mixed finite elements with velocity elimination for subsurface flow, *Journal of Computational Physics* 404 (2020) 109133, 23. doi:10.1016/j.jcp.2019.109133.
- [58] T. Barth, R. Herbin, M. Ohlberger, *Finite volume methods: foundation and analysis*, John Wiley & Sons, Ltd, 2017, pp. 1–60. doi:10.1002/9781119176817.ecm2010.
- [59] Y. Notay, Convergence analysis of perturbed two-grid and multigrid methods, *SIAM Journal on Numerical Analysis* 45 (3) (2007) 1035–1044. doi:10.1137/060652312.
- [60] X. Xu, C.-S. Zhang, Convergence analysis of inexact two-grid methods: a theoretical framework, *SIAM Journal on Numerical Analysis* 60 (1) (2022) 133–156. doi:10.1137/20M1356075.
- [61] Y. Saad, *Iterative methods for sparse linear systems*, 2nd Edition, Society for Industrial and Applied Mathematics, Philadelphia, PA, 2003. doi:10.1137/1.9780898718003.
- [62] J. Xu, L. Zikatanov, Algebraic multigrid methods, *Acta Numerica* 26 (2017) 591–721. doi:10.1017/S0962492917000083.
- [63] X. Xu, C.-S. Zhang, A new analytical framework for the convergence of inexact two-grid methods, *SIAM Journal on Matrix Analysis and Applications* 43 (1) (2022) 512–533. doi:10.1137/21M140448X.
- [64] S. Balay, S. Abhyankar, M. F. Adams, S. Benson, J. Brown, P. Brune, K. Buschelman, E. Constantinescu, L. Dalcin, A. Dener, V. Eijkhout, W. D. Gropp, V. Hapla, T. Isaac, P. Jolivet, D. Karpeev, D. Kaushik, M. G. Knepley, F. Kong, S. Kruger, D. A. May, L. C. McInnes, R. T. Mills, L. Mitchell, T. Munson, J. E. Roman, K. Rupp, P. Sanan, J. Sarich, B. F. Smith, S. Zampini, H. Zhang, H. Zhang, J. Zhang, *PETSc/TAO users manual*, Tech. Rep. ANL-21/39 - Revision 3.17, Argonne National Laboratory (2022).
- [65] M. A. Christie, M. J. Blunt, Tenth SPE comparative solution project: a comparison of upscaling techniques, *SPE Reservoir Evaluation & Engineering* 4 (04) (2001) 308–317. doi:10.2118/72469-PA.
- [66] X. S. Li, J. W. Demmel, SuperLU.DIST: A scalable distributed-memory sparse direct solver for unsymmetric linear systems, *ACM Transactions on Mathematical Software* 29 (2) (2003) 110–140. doi:10.1145/779359.779361.
- [67] V. Hernandez, J. E. Roman, V. Vidal, SLEPc, *ACM Transactions on Mathematical Software* 31 (3) (2005) 351–362. doi:10.1145/1089014.1089019.
- [68] M. Dryja, M. V. Sarkis, O. B. Widlund, Multilevel Schwarz methods for elliptic problems with discontinuous co-

- efficients in three dimensions, *Numerische Mathematik* 72 (3) (1996) 313–348. doi:10.1007/s002110050172.
- [69] I. Berre, F. Doster, E. Keilegavlen, Flow in fractured porous media: A review of conceptual models and discretization approaches, *Transport in Porous Media* 130 (1) (2018) 215–236. doi:10.1007/s11242-018-1171-6.
 - [70] J. W. Sheldon, J. Cardwell, W. T., One-dimensional, incompressible, noncapillary, two-phase fluid flow in a porous medium, *Transactions of the AIME* 216 (01) (1959) 290–296. doi:10.2118/978-G.
 - [71] H. L. Stone, J. Garder, A. O., Analysis of gas-cap or dissolved-gas drive reservoirs, *Society of Petroleum Engineers Journal* 1 (02) (1961) 92–104. doi:10.2118/1518-G.
 - [72] K.-A. Lie, An introduction to reservoir simulation using MATLAB/GNU Octave: User guide for the MATLAB Reservoir Simulation Toolbox (MRST), Cambridge University Press, 2019.
 - [73] D. Arnold, V. Demyanov, D. Tatum, M. Christie, T. Rojas, S. Geiger, P. Corbett, Hierarchical benchmark case study for history matching, uncertainty quantification and reservoir characterisation, *Computers & Geosciences* 50 (2013) 4–15.
 - [74] J. R. Wallis, Incomplete Gaussian elimination as a preconditioning for generalized conjugate gradient acceleration, Vol. All Days of SPE Reservoir Simulation Conference, 1983. doi:10.2118/12265-MS.
 - [75] J. R. Wallis, R. P. Kendall, T. E. Little, Constrained residual acceleration of conjugate residual methods, Vol. All Days of SPE Reservoir Simulation Conference, 1985. doi:10.2118/13536-MS.